DSR II, Special Issue I – Understanding ecosystem processes, timing, and change in the Pacific Arctic

Shifts in the physical environment in the Pacific Arctic and implications for ecological timing and conditions

Matthew R. Baker[a*], Kirill K. Kivva[b], Maria N. Pisareva[c], Jordan T. Watson[d], Julia Selivanova[b,c]

[a]*North Pacific Research Board, 1007 West Third Avenue, Anchorage, AK, 99501 USA*
[b]*VNIRO, Russian Federal Research Institute of Fisheries and Oceanography, 17 V. Krasnoselskaya, Moscow 107140 Russia*
[c]*P.P. Shirshov Institute of Oceanology, Russian Academy of Sciences, 36 Nakhimovsky Prospekt, Moscow 117997 Russia*
[d]*National Oceanic and Atmospheric Administration, Alaska Fisheries Science Center, Auke Bay Laboratories 17109 Pt. Lena Loop Road, Juneau AK 99801 USA*

ABSTRACT

The northern Bering Sea and Chukchi Sea represent the gateway from the Pacific to the Arctic. This contiguous marine system encompasses one of the largest continental shelves in the world and serves as the sole point of connection between the North Pacific and Arctic Ocean. This region has unique attributes and complex dynamics, driven by the convergence of distinct water masses, dynamic currents, advection between Pacific and Arctic systems, and important latitudinal gradients relevant to stratification and water mass structure, water temperature, and seasonal ice cover. Many processes and interactions in the region appear to be changing with important implications for both hydrography and ecology. Our analyses access remote and local data sources in US and Russian waters to characterize oceanographic conditions and analyze the implications of dramatic shifts in recent years. Previously, this region appeared resistant to trends apparent elsewhere in the greater Arctic. Now, the Pacific Arctic also appears to be in rapid transition. The conditions observed in 2017-2019 are unprecedented. We note important shifts in the phenology and magnitude of physical variables, including sea-ice extent, concentration, and duration, as well as extreme reduction in the extent and intensity of the related Bering Sea cold pool. We also note distinct regional dynamics in sea surface temperature in the Bering-Chukchi system, distinguishing western, eastern and northern areas of the Bering Sea. Specifically, our analyses distinguish the northern Bering Sea as an important transition zone between the Pacific and Arctic with higher frequency variability in sea surface temperature anomalies. Our results suggest that the strength and position of the Aleutian Low may be linked to warm to cold phases in the Bering Sea and has an important role in large-scale circulation. While cold winds out of the north are necessary to form ice in the northern Bering Sea, strong winds may be associated with weak sea ice, as wind action may break ice and enhance vertical mixing, counteracting enhanced sea-ice production from the advection of cold air. Research in this important region is complicated by international borders but may be enhanced through international collaboration. This analysis represents an attempt to integrate data across Russian and US waters to more fully represent system-wide processes, to contrast regional trends, and to better understand physical interactions.

Keywords: US, Russia, Bering Sea, Chukchi Sea, Marine system, Sea ice, Sea surface temperature, Hydrography, Water masses, Wind, Phenology, Climate, International collaboration

*Corresponding author.
E-mail address: Matthew.Baker@nprb.org (M.R. Baker)

1. Introduction

1.1. Pacific-Arctic system

The Pacific Arctic region, spanning the Bering-Chukchi complex (Fig. 1), encompasses the sole ocean conduit between the Pacific and the Arctic, linked by the narrow (85 km) and shallow (50 m) Bering Strait. Despite annual mean northerly winds (Woodgate et al., 2005), mean transport though the Bering Strait is 0.8 Sv northward (Sv, Sverdrup, is a non-SI unit of flow; 1 Sv = 10^6 m^3 s^{-1}; Ratmanov, 1937; Natarov, 1967; Coachman et al., 1975; Woodgate et al., 2005), though recent analyses indicate sustained increases (~1.2 Sv) in Bering Strait inflow to the Arctic (Woodgate 2018). Transport is highly variable and reversible with a range of -2 to 3 Sv (Roach et al., 1995). Northward transport of Pacific waters imports carbon, nutrients, and plankton into the Arctic (Asahara et al., 2012; Torres-Valdes et al., 2013); it also transports heat and has important influences on Arctic sea ice (Woodgate et al., 2010) and global hydrologic (Agaard and Carmack, 1989) and thermal-haline circulation (Hu et al., 2010). Throughout this region, there are important and distinctive north-south gradients. These latitudinal gradients, however, appear to be shifting with important implications for each regional system, as well as for broader Pacific-Arctic interactions. Each system in the study area is briefly described below.

1.1.1. Western Bering Sea and Basin

The western Bering Sea (WBS) shelf is narrow (40-130 km), extending from Cape Navarin in the north to the Commander Islands and southern Kamchatka Peninsula (Kivva, In Press). Flow is southward along the shelf break (Natarov, 1963), dominated by the East Kamchatka Current (referred to as the ‘Kamchatka Current’ in some literature), a western boundary current driven by gyre dynamics associated with the adjacent Bering Sea Basin (Verkhunov and Tkachenko, 1992; Verkhunov, 1995). This flow accelerates in winter (Nov-Mar) and slows in summer (May-Aug). In contrast to temperature gradients, salinity increases through the water column. The narrow WBS shelf has higher per-unit-area pelagic production, compared with other regions in the Bering and Chukchi seas (Aydin et al., 2002; Aydin and Mueter, 2007). The vertical structure in the WBS includes an upper mixed layer (0-25 m), cold intermediate layer (55-250 m), warm intermediate layer (250-500 m), and deep Pacific water mass (>500 m; Khen et al., 2015). The depth of convection depends on winter heat loss. The bottom of this active layer is deepest along the Kamchatka Peninsula (Luchin et al., 2007; 2009). North of Cape Navarin, flow drives northward to the Gulf of Anadyr, over the northern Bering Sea shelf and subsequently through the Bering Strait (Khen, Pacific Research Fisheries Center, TINRO, Vladivostok, Russia, personal communication). There are as many as 11 distinct water masses that converge in the area north of Cape Navarin (Danielson et al., 2011), including Bering Shelf Water, Anadyr Water, shelf and shallow basin waters, and coastal waters.

1.1.2. Eastern Bering Sea

The eastern Bering Sea is defined by a broad (~500 km wide) highly productive continental shelf that extends from the Alaska Peninsula to the Bering Strait, typically defined by three oceanographic depth domains (Inner: 0-50 m, middle: 50-100 m, and outer: 100-200 m). There is also a distinct separation north-south defined by temperature. A 'cold pool' of bottom water < 2°C extends southwards through the middle domain (Wyllie-Echeverria 1995; Wyllie-Echeverria and Wooster, 1998; Stabeno et al., 2016). This oceanographic feature represents the footprint of winter sea ice and usually persists throughout the summer. In warm years, the cold pool is restricted to the north. In cold years, it may extend to the Alaska Peninsula (Stabeno et al., 2012a). The cold pool serves as a barrier and thermal refuge to fish and invertebrate populations and contributes to a strong latitudinal gradient in physical dynamics and ecosystem structure (Mueter and Litzow, 2008; Baker and Hollowed, 2014; Ortiz et al., 2016). The southeastern Bering Sea (EBS) is a subarctic system with significant groundfish populations and significant pelagic and benthic energy pathways (Aydin et al., 2002; Aydin and Mueter, 2007). This is in stark contrast to the Arctic systems of the northern Bering Sea (NBS) and Chukchi Sea, which are dominated by benthic invertebrates and benthic energy pathways (Grebmier et al., 1988; Grebmier et al., 2006; Whitehouse et al., 2014). Previous studies have demonstrated that not only physical properties, but also species distribution and community composition are distinct in the EBS and NBS (Mueter and Litzow, 2008; Stevenson and Lauth, 2012; Baker and Hollowed, 2014) with the relative extent of each biogeographic area reflective of temperature regimes (Baker and Hollowed, 2014). While the conditions of the EBS shelf generally reflect a subarctic system, the cold pool of the middle EBS shelf more closely resembles an Arctic system

(Wyllie-Echeverria, 1995) and therefore represents a variable extension of Arctic conditions associated within the NBS into the EBS area.

1.1.3. Northern Bering Sea

The seasonally ice-covered NBS encompasses the continental shelf north of 60°N (Sigler et al., 2017), and includes areas north of the Anadyr River and Yukon River drainages (Andriashev, 1939). This system ranges from Russian coast in the west to the Alaska Coast in the east (Golikov et al., 1980) and north to the Bering Strait. Mean current flow is northward into the Arctic Ocean most of the year (Coachman, 1993; Danielson et al., 2014) and transport plays an important role in exchange and advection of production from the Pacific to Arctic (Panteleev et al., 2012). This ecosystem is characterized by distinct regional dynamics in wind stress and circulation, the integration of various water masses, fluctuating sea ice, highly seasonal production, and benthic-dominated trophic transfer (Grebmier et al., 2006). Historically, important differences in water column physics have been noted between the otherwise contiguous northern and southern sectors of the Bering Sea Shelf, with an Arctic-Subarctic temperature front (Stabeno et al., 2012b) and distinct nutrient loading (Kivva, 2016) at approximately 60°N. Until recently, the NBS has been more closely connected in hydrographic and biological characteristics to the Chukchi Sea to the north than to the southern portions of the Bering Sea (Walsh et al., 1997; Grebmier et al., 2006; Stabeno et al., 2012b; Sigler et al., 2017). Distinct attributes related to physical oceanography, biogeography, species distributions and community structure in the NBS, EBS and WBS are further detailed in Baker (In Press), Siddon (In Press) and Kivva (In Press).

1.1.4. Bering Strait

Northward flow is the defining hydrographic feature in the Bering Strait. Mean northward transport is caused by the pressure head between the Pacific and Arctic Oceans (Coachman and Aagaard, 1966; Woodgate et al., 2012) and wind effects. This transports a significant volume of freshwater (Aagard and Carmack, 1989; Woodgate et al., 2012) and heat (Woodgate et.al, 2007; Steele et al., 2008) and has strong influence on the circulation, physical processes and ecosystem structure of the Arctic (Pickart et al., 2005). Peak northward flow occurs in June-July. In the summer, warm fresh waters are at the surface, while in autumn, temperature inversion occurs with colder waters overlying warmer saltier waters. Homogenization occurs in winter as a result of wind-driven or flow-related mixing, convection due to heat fluxes, and brine rejection due to ice formation (Woodgate et al., 2015).

1.1.5. Chukchi Sea

The Chukchi Sea is an important transition region for Pacific waters entering the Arctic Basin (Pisareva, 2018). It is also one of the most productive areas of the world's oceans (Walsh et al., 2005). North of Bering Strait, seafloor topography directs flow along Herald Canyon in the west, Barrow Canyon in the east, and the Central Channel (Woodgate et al., 2005). Residence time and water properties are heavily influenced by the throughflow from the Bering Sea (Woodgate et al., 2015). These Pacific waters are detectable in parts of the upper Arctic Ocean (Steele et al., 2008) and influence recession of sea ice in the Arctic. In summer, Pacific Water adds subsurface heat. In winter, Pacific Water forms a protective layer between the winter sea ice and warmer Atlantic waters (Francis et al., 2005; Shimada et al., 2006; Woodgate et al., 2010).

1.1.6. Integrated Pacific-Arctic System

The systems within the Pacific Arctic region, while distinct, are strongly interconnected and trends in each should be considered in assessing northern hemispheric ecosystem change (Brown and Arrigo, 2012). Importantly, attributes that have historically distinguished these regions (particularly the thermal barrier between the southern and northern Bering Sea shelf), appear to be eroding at a rate and to an extent that far exceed predictions made only a few years ago (Stabeno et al. 2012b; Lomas and Stabeno, 2014).

1.2. Sea ice, cold pool and thermal regimes

Historically, the Bering Sea has been ice-free in summer and covered with extensive sea ice in winter, with mean maximum sea-ice extent in March (range=Jan-

Apr; Wendler et al., 2014). In winter, atmospheric forcing and ocean circulation drive a sea-ice advance that is unparalleled in the northern hemisphere (Sigler et al., 2010). The Bering Sea cold pool represents the summer footprint of this seasonal sea-ice cover. Recently there has been a series of distinct thermal phases recognized in the EBS (Stabeno et al., 2001; 2007; 2012a,b; 2017, Stevenson and Lauth, 2019). Following a period of high interannual variability (1982-2000), the system transitioned into multi-year stanzas of warm (2000-2005, 2014-2016) and cold periods (2007-2013). These trends (April-August) have also been recognized in the WBS (Glebova et al., 2009), related to negative temperature anomalies in 2006-2013 correlated with cold winters and extensive sea ice (Khen et al., 2013). Khen and Zavolokin (2015) also showed differences in circulation between 2002-2006 and 2007-2011 related to changes in spring sea level pressure (SLP) patterns and Kivva (In Press) notes that alternating cold (2006-2013) and warm (2000-2005, 2014-2016) phases were prevalent. A recent warm period initiated in 2014 throughout the Bering Sea, with 2014-2016 bottom temperatures well above the long-term mean (Conner and Lauth, 2017). In winter 2017-2018 the maximum extent of sea ice in the Bering Sea was the lowest on record.

1.3. Evidence of system change

In the past 50 years, the Arctic Ocean has experienced unprecedented and accelerating sea-ice loss (Walsh and Chapman, 2001; Stroeve et al., 2007; Cosimo, 2012), with predictions for an ice-free Arctic (summer minimum) by mid-century (Wang and Overland, 2009). Multiple factors are driving reductions in sea-ice extent, concentration, and duration, including rising air temperature (Lindsay and Zhang, 2005), increased flux of warm water into the Arctic (Maslowski et al., 2001), and advection of ice out of the Arctic (Serreze et al., 2007). This reduction of sea ice has also initiated positive feedbacks (Perovich et al., 2007). Until recently, these processes appeared absent in the Pacific Arctic, especially the Bering Sea (Brown et al., 2011; Brown and Arrigo, 2012).

Prior to 2017, no significant trend in sea-ice extent in the Bering Sea was evident and it was assumed that seasonal sea ice would continue to form in the NBS (Walsh et al., 2017). Oceanographic conditions observed in 2017-2019, however, contradict these assumptions. Reductions in extent and duration of sea ice were evident in the satellite record, with virtually no sea ice in the EBS in winter 2017-2018 (< 0.2 x 10^6 km^2) and winter 2018-2019 (< 0.4 x 10^6 km^2; Stabeno, et al. 2019). These conditions reflect the lowest sea-ice cover on record (Stabeno and Bell, 2019) and the first recorded absence of the cold pool. Shifts in salinity and nutrient dynamics (Stabeno et al., 2019), northward movement of sub-Arctic groundfish stocks (Stevenson and Lauth, 2019; Baker, 2020), and notable marine bird mortality events (Duffy-Anderson et al., 2019) were associated with these anomalous conditions. Pressing questions include whether this represents a phase or regime shift (Huntington et al., 2020) and the extent to which these processes and properties vary over decadal and interannual timeframes (Overland et al., 2012; Woodgate et al., 2015).

Documentation and analysis of trends and variability in sea ice are essential to project future trajectories and understand ecosystem implications (Walsh et al., 2017). The post-1979 satellite record provides insight into decadal variability. Our analysis explored this at various timeframes, comparing consecutive warm (2001-2005, 2014-2016) and cold (2007-2012) years, the preceding period of interannual variability (1982-1999), and recent anomalous conditions (2017-2018).

1.4. Integrated research and international coordination

Scientific access across the Bering-Chukchi complex is complicated by the political boundary between the United States and Russia (Kinney et al., 2014). Nevertheless, this region is also an area of active research for many Arctic states, including US, Russia, Japan, Korea, China, and Canada. Several international marine research and management organizations have been active in the region, including the Arctic Council, International Arctic Science Committee (IASC), North Pacific Marine Science Organization (PICES), Intergovernmental Consultative Committee (ICC), Ecosystem Studies of the Subarctic and Arctic Seas (ESSAS), and Pacific Arctic Group

(PAG) (Van Pelt et al., 2017). Directed collaborative research between the US and Russia has occurred in the form of coordinated cruise transects in the long-term ecological investigations of the Bering Sea and other Pacific Ocean ecosystems (BERPAC, 1998-1995; Grebmier et al., 2006) and the Russian American Long-term Census of the Arctic (RUSALCA, 2004-2011; Crane and Ostrovskiy, 2015; Pisareva, 2015), joint mooring deployments (Woodgate et al., 2015), US-Russian cooperative surveys in the NBS and Gulf of Anadyr (1990; Sample and Nichol, 1994), Bering Aleutian Salmon International Surveys (BASIS), https://npafc.org/working-groups/#basis), and in the North Pacific Research Board (NPRB) Arctic Integrated Ecosystem Research program (Arctic IERP; Baker et al., 2020).

Our analysis is part of an ongoing attempt to integrate scientific data from Russian and US surveys and moorings with region-wide satellite coverage to: (1) highlight recent trends relative to historical baseline conditions; and (2) investigate potential mechanisms and implications for the dramatic shifts in the physical conditions of this important Pacific-Arctic gateway. Observations are informed by research supported by NPRB, US National Oceanic and Atmospheric Administration (NOAA), Russian Federal Research Institute of Fisheries and Oceanography (VNIRO) and by discussions and exchange at the 2016 and 2017 PICES workshops on data sharing in the Northern Bering Sea (Eisner et al., 2017; Baker et al., 2018) and North Pacific Ecosystem Status Report (https://meetings.pices.int/projects/npesr).

2. Data and methods

Our analyses consider data at various resolutions and spatial scales, consistent with different sources of remote sensing and in situ data. We examine sea ice, sea surface and bottom temperature data along north-south gradients within the Bering Sea and Chukchi Sea complex. We also examine east-west gradients, use patterns in sea surface temperatures (SST) to identify areas of statistical convergence and differentiation, and examine the influence of wind and atmospheric processes. We then apply these results to identify sub-regional patterns in the shelf-basin system and to provide insight as to how regional properties influence system-scale processes.

2.1. Regional delineation of the Pacific Arctic – cluster analysis

2.1.1. Data

To evaluate the entire Bering-Chukchi Sea complex (50-76°N, 162E-156°W), the NOAA Optimum Interpolation Sea-Surface Temperature V2 monthly data product was used. This dataset has spatial resolution of 1°×1°, with temporal coverage from 1981 to present (https://www.esrl.noaa.gov/; Reynolds et al., 2002). Data for complete years from 1982-2018 were used in our analysis. Clustering was performed to group grid nodes with similar variability in sea surface temperature anomalies (SSTA). Correlation was chosen as a measure of similarity instead of Euclidian distance. This allowed us to group grid nodes with similar SSTA dynamics (patterns over time), rather than absolute values, and delineate regions of synchronous SSTA. The dimensionality of the initial data was 860 × 444 (grid nodes × monthly SST or SSTA values). Annual mean SSTA values were calculated to reduce dimensionality of the data. Monthly SST values were averaged over every year (1982-2011) and the 30-yr mean was calculated for every grid node. This 30-year mean was subsequently subtracted from annual mean SST time-series for every grid node. Data normality was checked with the Shapiro-Wilk test. Annual mean SSTA values of many grid nodes for 1982-2011 could not be treated as normally distributed (160 of 860 data points had W-values < 0.927 with p-values < 0.05). Data were positively skewed in areas close to Cape Navarin, Cape Olyutorsky and Karaginsky Gulf and negatively skewed in Norton Sound. Areas north of 72° N were covered by sea ice almost permanently until recent years. This resulted in SST values (SST = –0.4 to +0.1 °C) close to the freezing point for sea water (SST ~ –1.7 °C) in most of the time series, whereas many grid nodes in this area were seasonally ice-free in recent years (SSTA = +0.5 to 1.0 °C). To account for this skewed distribution, we used the non-parametric Spearman correlation coefficient.

2.1.2. Clustering approach

The DBSCAN algorithm (Density-Based Clustering for Applications with Noise; Ester et al., 1996) and the “dbscan” package in R [https://cran.r-project,org/web/packages/dbscan/dbscan.pdf] were used to identify clusters of similar SSTAs for grid cells in the Bering-Chukchi regions. This approach searched for data points with more than N nearest neighbors (‘minPts’) within a certain radius (ε, ‘eps’). Those data points are assigned ‘core points’. All neighbors of core point within ε radius were considered to belong to the same cluster (‘direct density reachable’ points). The DBSCAN result depends on the choice of eps and minPts parameters and should balance the signal to noise ratio (Schubert et al., 2017). For our purpose, we limited ‘noise’ to values between 0.1-0.3. We performed clustering for all combinations of minPts between 5-70 and eps between 0.04-0.18 with step 0.02 and documented the number of clusters and noise ratio for every combination (Appendix, Fig. A-1), and visualized all results (Appendix, Fig. A-2, A-3). Results were similar and we choose minPts=31 for subsequent analysis and set eps=0.1. Data included 1982-2018 (444 months). Clustering was based on annual SSTA values as it was difficult to perform clustering on monthly values without dimensionality reduction.

2.1.3. Regional monthly SSTA calculation

Regional SSTA values (1982-2018) were calculated as the monthly value minus mean value for the month of interest from a 30-year baseline reference period, excluding periods of recent warming (1982-2011). This allowed us to remove variance related to seasonal cycle and focus on relative cold and warm events. The SSTA time series were averaged across every region, weighting by the cosine of the latitude of the grid nodes. The annual SSTA values were calculated as January-December means. All months were divided into five categories based on the standard deviation (SD). Months with absolute SSTA values > 2SD were considered extremely cold or extremely warm (depending on the sign of SSTA value). Absolute SSTA values between 1 SD and 2 SD were classified as cold or warm, and months with values between -1SD and +1SD were considered normal.

2.2. Bering Sea – sea surface temperature

To evaluate regional differences at higher resolution within the Bering Sea, SST data from the NOAA Coral Reef Watch version 3.1 operational global satellite (pacioos.hawaii.edu/metadata/dhw_5km.html) were applied. Data were accessed via the Pacific Islands Ocean Observing System ERDDAP site (https://pae-paha.pacioos.hawaii.edu/erddap/index.html) and spanned 01 January 1986 – 31 December 2019. These data include daily satellite information with a 5-km spatial resolution. Data were spatially apportioned to the EBS, NBS, and WBS using the PICES NPESR Working Group 35 spatial boundaries for regions 13, 14, and 16, respectively (https://meetings.pices.int/projects/npesr). Because we were primarily interested in shelf habitats, data were limited to locations with depths between 10 m and 200 m, as determined from Amante (2009), accessed via the *marmap* package (Pante and Simon-Bouhet, 2013) in R. The spatial extent of each system (EBS, WBS, NBS) as defined for this analysis is shown in the Appendix (Fig. A-4). Seasonal components were removed from time series using an additive decomposition with a frequency of 365 using the *fpp2* package (Hyndeman and Athanasopoulos, 2018) in R Statistical Software (version 3.5.0). In addition to an analysis of trends in the time series of the EBS, NBS, and WBS during different climatic phases (e.g. warm, cool), we also directly compared the EBS and NBS, decomposing the time series as a reflection of their difference in temperature.

2.3. Sea-ice concentration

Sea-ice concentration (SIC) data were obtained from the Climate Data Record (CDR) of the National Snow and Ice Data Center (NSIDC) (Meier et al., 2017a). Data were derived from Special Sensor Microwave Imager (SSM/I) and Special Sensor Microwave Imager and Sounder (SSMIS) passive microwave radiometers and processed with a bootstrap algorithm (Peng et al., 2013). CDR is currently limited to the years 1979-2017. Version 1 of the near-real time Climate Data Record (NRT-CDR) was used for 2018 (Meier et al., 2017b). This product is based on SSMIS data, produced using bootstrapping and NASA algorithms. Both data sets are based on the polar stereographic grid of nominal resolution 25 × 25 km.

2.4. Sea-ice retreat

Similar to many previous studies, we used the SIC threshold approach to define the date of sea-ice retreat (DOR) (e.g. Stroeve et al., 2016; Lebrun et al., 2019). Different thresholds (e.g. 0.15, 0.30, and 0.50 fractional areal coverage) revealed similar results in previous studies; we chose 0.15 as a threshold. Data were smoothed by a 7-day running mean to filter out high-frequency synoptic variability, following Peng (2018). While most previous studies used the first day when SIC fell below the threshold level as the DOR, our study focused on how changes in physical environment may alter biological processes. Thus, we determined the best metric to signal the shift to an ice-free state would be the last date on which SIC reached the 0.15 threshold.

2.5. Ice extent and open water index

Areal extent of open water in the Bering Sea and Chukchi Sea was calculated using the National Snow and Ice Data Center [https://nsidc.org/data] regional monthly sea ice data index [Sea Ice Index Regional Monthly Data G02135_v3.0], using 15% SIC. Data were compiled using passive microwave estimates of Arctic sea-ice extent (1979-present). Regional extent for the Bering Sea and Chukchi Sea were comprehensive and defined by the NSIDC (https://nsidc.org/data/masie/browse_regions; Appendix, Fig. A-5). In the Bering Sea, our index of interest was the extent of sea-ice coverage. We measured sea ice at a standard reference date of March 15 (approximate mid-point for the timeframe of mean annual maximal ice extent in February-April; Appendix, Fig. A-6). We calculated an annual index of open water as a function of the deviation of March 15 ice extent in each year from maximum March 15 sea-ice extent in the timeseries. In the time series, maximum sea-ice extent occurred in 2012 (817,752 km^2). In the Chukchi Sea, our interest was spring melt and the location of ice edge at peak primary production. We used a standard reference date of May 15, which historically coincides with the initiation of sea-ice retreat, the onset of open water production (Wang et al., 2005; Zhang et al., 2015), and chlorophyll a (chl-a) maximum associated with under-ice blooms (Brown et al., 2015). We calculated open water as the difference between the full areal extent of Chukchi Sea (800,000 km^2) minus the areal extent of sea ice within that that region on May 15. Regression analyses were performed in SigmaPlot (Systat Software). All other statistical applications were applied using R statistical computing software (R Development Core Team 2019).

2.6. Bering Sea cold pool

The annual extent of the Bering Sea cold pool (bottom temperatures ≤ 2 °C; Stevenson and Lauth, 2019; Thorson, 2019) was estimated via data collected in the annual NOAA bottom trawl surveys of the EBS and NBS conducted during the summer months of 1982-2018 (Stevenson and Lauth, 2019). In all years, the survey covered the EBS shelf from the Alaska Peninsula to approximately 61°N. Surveys conducted in 2010, 2017 and 2018 also encompassed US waters within the NBS. Bottom water temperatures were recorded using a Sea-Bird SBE-39 datalogger (Sea-Bird Electronics, Inc., Bellevue, WA) attached to the trawl headrope. Bottom temperatures were recorded at each survey station. Maps of the cold pool area were developed in ArcGIS using Inverse Distance Weighting (IDW) interpolation. Statistical analyses were developed in R statistical computing software (R Development Core Team 2019). Differences in the areal extent of the cold pool were assessed using analysis of variance (ANOVA) and Tukey's HSD test on pairwise comparisons.

2.7. Sea surface pressure and wind vectors

Composite maps of mean sea level pressure (SLP) fields and 10-m winds were constructed for winter months (November - March) with the use of 1 h ERA5 atmospheric reanalysis with 0.25° spatial resolution. The ERA5 reanalysis data were downloaded from the European Centre for Medium-Range Weather Forecasts (ECMWF) website https://www.ecmwf.int/en/forecasts/datasets/archive-datasets/reanalysis-datasets/era5.

3. Results

3.1. Delineation of regions in the Pacific Arctic

To identify regional boundaries according to patterns in mean monthly SSTA, we set the minPts parameter of DBSCAN to 31 and varied the eps parameter to choose the best spatial organization of clusters and minimize noise. Setting eps=0.12 resulted in three clusters with noise ratio of 0.18 (Fig. 2a, left plot). A decrease in eps (eps = 0.10) resulted in an increase of the noise ratio and a simultaneous decrease of cluster areas (Fig. 2a, center plot). Further reduction in eps values resulted in the separation of the Chukchi-Siberian cluster into two clusters with an increase in noise to 0.4 (Fig. 2a, right plot). Values of eps between 0.1334-0.1344 resulted in collapsing three clusters into two clusters (Appendix A, Fig. A-2), and eps > 0.1345 resulted in only one cluster with very few points assigned as 'noise'. Results for eps of 0.08-0.12 reflected meaningful physical boundaries. Areas north of Bering Strait usually experienced more severe ice conditions (i.e. higher concentrations, greater ice thickness, and longer duration of ice cover) than other regions. Due to more extensive ice cover, annual mean SSTs were low and interannual variability was lower than south of Bering Strait. With certain variables, the area of the Chukchi and East-Siberian seas (CS-ESS) divided into two clusters roughly along the boundary between those two seas. This is probably a reflection of different processes controlling thermal conditions in each sea; the Chukchi Sea is more strictly controlled by the inflow of the warm Bering Sea waters than the East-Siberian Sea. Overall, the DBSCAN cluster analysis identified separate regions within the Bering-Chukchi complex, according to distinct patterns in thermal dynamics (epsilon radius = 0.10; nearest neighbor minPts = 31). All combinations of eps and minPts resulted in the separation of the Bering Sea into at least two clusters: western, and eastern. Larger eps values resulted in closer geographic location of margins of those clusters, while lower values led many of those grid nodes to be assigned as 'noise'. The NBS (areas north of 60 °N) included areas assigned as 'noise' in the

DBSCAN analysis. Those 'noise' regions were treated as a transition area between neighboring clusters. It is anticipated that NBS SSTA variability may at times match patterns of variability in the EBS, but at other times match patterns of variability in the Chukchi Sea, depending on atmospheric and marine circulation. In the final analysis, Region 4 is identified as the remaining grid nodes of this region assigned as 'noise' (Fig. 2b).

3.2. Regional patterns in SSTA in the Pacific Arctic

The final evaluation of SSTA variability 1982-2011 distinguished regionally coherent patterns in the CS-ESS, WBS, and EBS. We also identified the NBS as the area of high variability between 60-66 °N and 175°E -165°W (Fig. 2b). The NBS is a region of higher spatial and temporal SSTA variability and may be treated as transition region between three other regions. The CS-ESS region had generally low SSTA values, but anonymously warm spring-autumn conditions since 2016. The WBS and EBS regions behaved similarly, but with very different duration of cold/warm periods. For instance, 1998-2002 were substantially colder in the WBS, but only 1999 was cold in the EBS (2007-2012 were quite cold in the EBS, but only 2012 was cold in the WBS). Detailed results on each system are provided below.

3.2.1. Region 1 – CS-ESS

The north (CS-ESS) SSTA cluster (region1; Fig. 3, panel 1) exhibited little variability in SSTA in winter months because ocean water annually reaches the freezing point and SSTA values are therefore relatively constant. The highest interannual and within-region SSTA variability is seen in this region during summer. The SSTA time-series in this region may be roughly divided into three intervals: 1982-1989, 1989-2003, and 2004-2019. Before 1989, summer SST values were similar to winter values (e.g. the freezing point). This resulted in low SSTA values compared to later intervals. Between 1989 and 2003 many areas in the region started to experience ice-free conditions which resulted in warmer SST and positive SSTA values. At the same time, most of the northern part of the cluster was still ice-covered even in summer.

Exceptions occurred in 1990, 1993, and 1997, where SST values in most of the region were above the freezing point, which resulted in positive summer SSTA values. Since 2003, summer SSTA values have been mostly positive, with exceptions of high variability in the summers of 2006, 2008, and 2012-2013. Since 2004, the frequency of monthly SSTA values larger than the monthly standard deviation for the time series has increased, with several extremely warm months in spring and autumn.

3.2.2. Region 2 – WBS

Several distinct thermal regimes were observed in the WBS (region 2; Fig. 3, panel 2). Normal-cold conditions characterized the early time series (1982-1995) followed by several warm years (1996-1998), cold conditions (1999-2002), and then a prolonged warm phase (2003-2019) with a slight deviation toward colder conditions in 2012. The most extreme monthly temperatures in both warm (1996-1998) and cold (1999-2002) periods occurred in winter and spring. This suggests that winter-spring SST conditions may determine the thermal regime for the year (e.g. if winter/spring conditions are cold, the rest of the year will likely also be cold). Since 2003, warm conditions have predominated in the WBS, with few exceptions, though with large inter-annual SSTA variability. Mean annual SSTA values for all years except 2009 and 2012 were positive, and many months exhibited extremely warm conditions, particularly in summer. Since 2017, winter and spring conditions have been extremely warm. Thus 2003-2016 may be viewed as a period of variable warm conditions with a transition to extremely warm conditions in 2017-2019.

3.2.3. Region 3 – EBS

The EBS exhibited patterns in SST variability similar to the WBS, but with substantially shifted margins for the time intervals (region 3; Fig. 3, panel 3). Moreover, while the range of variability was similar in the WBS and EBS prior to 2006, the very cold period in the EBS (2007-2013) had no analog in the WBS. In the EBS, years 1982-1999 were highly variable without a distinct pattern, characterized by a series of transitions from relatively cold to relatively warm conditions with most monthly SSTA values falling between 0 ± 1 SD. This situation changed in 2000, followed by a relatively warm phase

(2001-2005), a cold phase (2007-2013), and subsequent warm phase (2014-2019). In contrast to the WBS region, the EBS region exhibited extremely warm conditions in both winter and spring, starting in 2015.

3.2.4. Region 4 – NBS

According to our analysis, the NBS is a region of 'noise' meaning all grid nodes there experienced SSTA dynamics that substantially differed both from the dynamics of any grid node in previously described areas (regions 1-3) as well as from the dynamics of any neighboring nodes within this 'noise' region (region 4). While monthly regional mean SSTA in the WBS and EBS exhibited a series of cold-to-warm transitions, dynamics in the NBS exhibited higher frequency variability, on the scale of months (region 4; Fig. 3, panel 4). This is a region of high inter-annual temporal and within-cluster spatial SSTA variability. Still, patterns reflect those observed in other regions with relatively warm (2001-2003, 2014-2019) and cold (2008-2012) phases. This region may be characterized as a transition region with substantially higher spatial-temporal SST variability.

3.3. Identification of distinct climatic phases via SST

High-resolution satellite-based SST data confirm a sequence of distinct phases in the Bering Sea (Fig. 4, top panel). In the EBS, a period of high interannual variability (1987-2000), transitioned into multi-year stanzas of warm (2000-2005, 2014-2016, 2017-2019) and cold periods (2006-2013). These trends were roughly mirrored in the NBS (though see differences between EBS and NBS sea surface temperatures; Fig. 4, bottom panel). Trends in SST differed substantially in the WBS. Alternating cold and warm phases were also prevalent, but according to a different pattern, such that the temporal bounds of these thermal phase shifts were offset. The WBS was characterized by relatively warmer temperatures in 1996-1998 and 2003-2016, colder temperatures in 1999-2002, and anomalously warmer temperatures in 2017-2019. In general, the WBS is colder than the EBS, though temperatures converged in 1996-1998 (warm period in the WBS) and 2006-2013 (overlap of a warm period in the WBS and a cold period in the

EBS). Since 2014, the water column 0-100m in the WBS has been warmer, relative to 1950-2003. In all sub-regions of the Bering Sea (EBS, WBS, NBS), the conditions of 2017-2019 exceeded values observed in the recent warm stanzas and represent the warmest conditions in the historical record in each respective system (Fig. 4, upper panel). It should be noted that the relative increase in temperature in this recent warming period (2017-2019) was greatest in the NBS. This is reflected in the reduced temperature differential between the EBS and NBS in this timeframe (Fig. 4, lower panel). In both 2006-2013 and 2017-2019, the difference in mean SST values between the EBS and NBS was reduced. In the former period (2006-2013), this was due to cold phase in the EBS, such that conditions in the EBS more closely resembled those typical of the NBS. In the later period (2017-2019), this reflects warming in both systems, but greater relative warming in the NBS, such that the conditions in the NBS more closely resemble those typical of the EBS.

3.4. Annual sea-ice extent and concentration

Analysis of the relationship between maximum annual sea-ice extent and a standardized annual index of sea-ice extent on March 15 suggested that the seasonal timing of maximum sea-ice extent varied greatest in years of greatest extensive sea-ice extent; the relationship was strongest in the timeframe of warm and cold phases analyzed (2000-2019, R^2=0.57, P<0.001; Appendix, Fig. A-6). It should be noted that mid-March was used to develop a standardized index of annual ice extent and that the seasonal timing of maximum ice extent will vary between years. Also, while mid-March sea-ice extent is well correlated with maximum ice extent, it is a significant underestimation. This standardized index was used to examine patterns of change in sea-ice extent over the timeseries, 1979-2018 (Appendix, Fig. A-7). Sea-ice extent and configuration varied greatly over this period with mid-March sea-ice extent ranging 55°N-60°N in the EBS (Alaska Peninsula to north of Nunivak Island) and 60°N-63°N in the WBS (south of Cape Olyutosky to north of Cape Navarin). There was extensive retreat in sea-ice extent in the Gulf of Anadyr in recent years (2017-2018). Maximum mid-March Bering Sea ice extent was observed in 2012 (2937×10^3 km^2); minimum mid-March Bering Sea ice extent was observed in 2018 (2318×10^3 km^2). The marginal ice zone (areas with sea-ice concentration 15% to 80%; http://seaiceatlas.snap.uaf.edu/) was highly variable; its greatest mid-March extent was observed in 1984 (332×10^3 km^2) and lowest in 2016 (125×10^3 km^2). While there were no significant trends in total mid-March sea-ice extent 1979-2018, the area of the marginal ice zone exhibited a steady decrease over the 40 years' period (-13.6% per decade). Mean sea-ice extent on March 15 in each of the climatic stanzas identified in this analysis was visualized (Fig. 5); the greatest sea-ice extent occurred in the EBS cold period 2006-2013 (2738×10^3 km^2), versus reduced areas in the EBS 2000-2005 (2500×10^3 km^2) and 2014-2016 (2573×10^3 km^2) warm periods.

The western part of the Bering Sea is consistently less ice covered in winter than the eastern shelf. Sea ice covers only a narrow coastal band along the Koryak and Kamchatka coasts. Sea ice starts to form in the Gulf of Anadyr in the middle of October. Outside the Gulf of Anadyr, sea ice forms in the embayments of the Koryak coast (Cape Olyutorsky to Cape Navarin) and inner part of the Korfa Bay in mid-November. In December, the rate of ice growth accelerates and peaks in February (Plotnikov and Vakulskaya, 2012). The area is totally ice free by the middle of June. In cold years (e.g. winter of 2011-2012) sea-ice growth may continue until the end of April. In contrast, ice cover in warm years (e.g. winter of 2002-2003) starts to disappear in February. Interannual variability of mean sea-ice cover of the western portion for the Bering Sea (WBS extent shown; Appendix, Fig. A-4) generally mimics that for the total Bering Sea ice cover (correlation coefficient, R=0.6, P<0.001; Gennady Khen, personal correspondence; Kivva, 2020).

3.5. Annual sea-ice retreat

The date of sea-ice retreat (DOR) was highly variable during the 40-year period (Appendix, Fig. A-8). Ice melt initiated in the end of February and was complete by the end of August. Mean DOR was May 22 in the Bering Sea and July 20 in the Chukchi Sea. The trend in mean day of spatial retreat in the Bering-Chukchi complex was positive (6.5 days later per decade). Mean DOR for sea ice in each of the identified climatic stanzas was visualized (Fig. 6). For annual areal extent in ice retreat timing in the Bering and the Chukchi Sea, see supplementary figure (Appendix, Fig. A-9).

3.6. Ice extent and open water

Differences in the annual areal ice extent are apparent and differences are notable between the warm, cold, and variable periods (Fig. 7, Table 1). As a consequence, the areal extent of open water in the Bering Sea on March 15 and in the Chukchi Sea on May 15 varied considerably across the time series (Fig. 8). Differences in the extent of open water were noted across identified climatic stanzas (Fig. 9; Table 1) in both the Bering Sea (ANOVA, $F_{4,36}$=2.63, P<0.001) and Chukchi Sea (ANOVA $F_{4,36}$=6.67, P<0.001).

3.7. Annual areal coverage of the Bering Sea cold pool

Annual areal extent of the cold pool varied across the time series (Fig. 10, Table 2) and differences were noted between climatic stanzas (1982-1999, 2000-2005, 2006-2013, 2014-2016, 2017-2018; ANOVA $F_{3,33}$=2.89, P=0.001). Post Hoc tests (Tukey HSD) noted significant differences between warm (2000-2005, 2014-2016) and cold (2006-2013) years (P<0.022). The cold period was also distinct from the 1982-1999 variable period (P=0.081). No differences were noted between recent warm periods (2000-2005, 2014-2016, P=0.999), nor between warm years and the variable period (1982-1999; P>0.555). The most recent anomalous year, 2018, was significantly different from both the cold period 2006-2012 (P=0.013), as well as the initial part of the timeseries,1982-1999 (P=0.038). As the cold pool may be defined at different temperature thresholds, we also examined differences in the mean areal extent of the cold pool between climatic stanzas, as defined as bottom temperatures colder than 2°C, 1°C, 0°C, and -1°C; all were significant (P<0.046). The most recent year of analysis (2018) had an extreme reduction in cold pool extent. Cold pool areal coverage as a percentage of the total survey area declined from a mean of 38.7% (1982-2018) to 1.4% in 2018. Temperatures within the cold pool were also warmer than previously observed;

no area in the 2018 survey had bottom temperature < 0°C, compared to a mean coverage of 11.7% for bottom temperatures < 0°C 1989-2018 (22% in cold years, 2006-2013; 5-6% in warm periods, 2000-2005 and 2014-2018). No temperatures < 1°C were observed in the NOAA EBS survey area in 2018, a phenomenon not previously observed.

3.8. Climate and wind

Mean composite winter SLP and wind patterns for November-March provide further insight into mechanisms (Fig. 11). In each of the warm periods (2000-2005, 2014-2016), both the Aleutian Low and the high-pressure system of Beaufort High and Siberian High were strong, with Aleutian Low located over the Aleutian Islands. These time intervals also exhibited slightly enhanced winds. In the later warm period (2014-2016), the Aleutian Low shifted to the east, altering the direction of the wind field over the islands. Alternatively, in the cold phase (2006-2013), while the high-pressure system still developed, the Aleutian Low was much weaker, with two centers - one in the Gulf of Alaska, another close to Russia. This resulted in weaker winds over the central Bering Sea, while the winds in the southeastern part of the EBS shelf were slightly enhanced, due to the longitudinal shift of the Aleutian Low. In the most recent period of anomalous warming (2017-2018), there was a significant shift of the Aleutian Low towards Russia, and prominent weakening of both systems. Composite annual SLP and winter wind anomalies (Fig. 12) demonstrate the substantial difference between 1979-2018 climatology and 2017-2018, including both the position shift and weakening of the Aleutian Low.

4. Discussion

4.1. New state of the Pacific Arctic

While sea-ice extent, concentration and duration has exhibited extensive reduction in the broader Arctic Ocean (Walsh and Chapman, 1990; Chapman and

Walsh, 1993; Levitus et al., 2000; Rigor and Wallace, 2004; Nghiem 2007; Kinnard et al., 2011; SWIPA 2011; 2012) and in the Chukchi Sea (Wood et al., 2015), the same trend had not been evident in the Bering Sea (Wendler et al., 2014; Peng et al., 2018). Including more recent data (2014-2018), particularly 2017-2019, however, alters that perspective. Both models and observations note increasing sea-ice loss, decreasing sea-ice thickness, shorter duration, and reduced extent of ice coverage in this region. This suggests a new state of the Pacific Arctic. The shift in pressure and weather patterns and the associated shift in sea-ice dynamics (Stabeno and Bell, 2019) have altered the timing and magnitude of heat exchange in this region. One result is that the thermal barriers (e.g. cold pool) previously evident in the Bering and Chukchi shelf have eroded. This has important implications for connectivity between Pacific and Arctic systems.

4.2. Phase shifts

The North Pacific is known as a region of decadal variations (Mantua et al., 1997; Overland et al., 1999; Di Lorenzo et al., 2008). Decadal variability is also apparent in the Bering Sea ice record, including historical analyses that extend to the 1800s (Walsh et al., 2017). Such variability is expected to continue in the future (Hollowed et al., 2013). The Bering Sea differs from the high Arctic in that its sea-ice cover is seasonal. Phases identified in our analysis match those of other studies of the region (Barbeaux and Hollowed, 2017; Stabeno et al., 2017). In the period 2000-2006, the EBS was characterized by reduced sea ice and above average ocean temperatures, while in 2007-2013, it was characterized by extensive ice and below average ocean temperatures. In the period 2014-2016, there was another shift to reduced sea ice and above average temperatures. Recent conditions (2017-2019) exceed anything witnessed in the historical record. Still, ice cover in the current winter (2019/2020) has been more extensive (more like a "cold year"). It is uncertain whether recent conditions represent an anomaly or the start of a fundamental transition (Stevenson and Lauth, 2019; Huntington et al., 2020).

4.3. Sea ice

Sea ice is the dominant driver of physical conditions in the Bering Sea. Historically, sea ice begins to form on the northern shelf in December with strong cold northerly winds, advecting ice southward (Pease, 1980). In years with limited sea ice on the southern Bering Sea shelf (2001-2005, 2014-2018), depth-averaged temperature was correlated to the previous summer ocean temperature (Stabeno et al., 2017). Winter sea ice had been expected to continue to form in the NBS and Chukchi Sea and a summer cold pool had been expected to form at depth (Stabeno et al., 2012a; Hollowed et al., 2013). In these systems, timing matters, both for ice arrival and retreat. A late ice arrival allows less time for ice formation and advection south. This alters both the influence and the character of the ice. The Chukchi has been freezing ~0.7 days later per year on average (1920-2019; Stabeno et al., 2019). In the NBS, no trend had been apparent through 2014. Recently (2014-2019), however, this region has also been freezing later (Stabeno et al., 2019). As the NBS begins to warm and reflect patterns evident in the greater Arctic, this will have important implication for other areas within the Bering Sea.

4.4. Sea surface temperature and cold pool

Oceanographic conditions observed in 2017-2019 are unprecedented. On the northern Bering Sea shelf, there was a near-complete lack of sea ice and no sea ice in the southeastern shelf in the winter 2017-2018 and in winter 2018-2019. Consequently, there was almost no cold pool in summer 2018 (Stabeno and Bell, 2019). To monitor bottom temperatures and to continue comparisons of cold pool areal extent, regular extension of surveys to northern areas are required. Research should continue to focus on important and complex dynamics related to the extent and timing of sea-ice cover, wind and stratification dynamics. While winters 2016-2017 and 2017-2018 were both warm, there was extensive, if weak, cold pool extent in summer 2017 due to a late winter freeze.

4.5. Salinity and stratification

Lack of sea ice has implications for stratification. In winter (Dec-Apr) the water column is uniformly cold. In spring ice melt develops a cold low-salinity layer at the surface that then gradually warms over the summer, in isolation from the bottom cold layer. In fall, storms and cooling breaks the stratification. Both salinity and temperature contribute to this dynamic. Without ice melt, there will be a reduced salinity gradient and thus weaker stratification; bottom temperatures may warm over the summer due to reduced stratification. Winter 2018 had the lowest ice year on record in the Bering Sea, primarily because of warm, southerly winds (Stabeno and Bell, 2019). Reduced sea ice resulted in warmer bottom temperatures and weaker stratification allowed warming of the bottom water during summer. The extreme reduction of the cold pool in 2018 may be partially explained by this increased mixing at depth due to the lack of salinity (Stabeno and Bell, 2019).

There are several indications that these conditions may be more prevalent in the future. Regional oceanographic models predict the reduced footprint of the Bering Sea cold pool observed in 2018 may be typical rather than anomalous by mid-century (Hermann, unpublished data). Winds out of the south are predicted to increase (Stabeno, unpublished data), setting conditions similar to those observed in 2017-2018. Conditions in the Chukchi Sea will also have implications for the Bering Sea. Delays in freezing in the southern Chukchi may delay freezing in the NBS, which in turn may reduce the time available for sea ice to be advected southward (Stabeno, personal communication).

4.6. Mechanisms for reduced sea ice and elevated temperatures

While the trends seem clear, the mechanisms and interactions are complicated. Physical conditions are governed by exchange between the ocean and air masses of Arctic and Pacific origin, advection from the Pacific to the Arctic, formation and retreat of sea ice, related stratification and mixing dynamics, and redistribution of water masses. Heat flux through the Bering Strait and Chukchi shelf appears to influence not only the distribution, but also the thickness of sea ice (Coachman et al., 1975; Shimada et al., 2006; Woodgate et al., 2010). The dominant parameters that control winter sea-ice extent in the Bering Sea are wind and air temperature, with persistent northerly winds in winter and spring leading to extensive sea ice (Stabeno et al., 2017). The factors recognized as contributing to the rapid loss of sea ice in the Arctic include warmer air temperatures (SWIPA 2011), wind forcing (Rigor et al., 2002; Ogi et al., 2010), radiative forcing (Francis and Hunter, 2007; Perovich et al., 2007) and oceanic heat flux from below (Shimada et al., 2006; Polyakov et al., 2011). Until recently, the Bering Sea has appeared exempt from loss of sea ice. Sea ice in the Bering Sea 1979-2012 had, until recently, demonstrated an increasing trend (Parkinson, 2014). Weather patterns in November 2017 through early January 2018 were unusual, most notably the duration of the southerly winds. While ice extent during winter months in 2017-2018 was well below previous years, early in the 2018-2019 ice season, ice extent was near normal, only declining to record lows after January. The interplay between air temperatures and wind direction has important implications and trends in this region will have influence beyond the Pacific Arctic. Transport of Pacific waters into the Arctic Ocean play an important role in the exchange of properties between these two systems (Pantleev et al., 2012) and freshwater inflow from the Bering Sea into the Chukchi Sea is an important influence on stratification and maintenance of the Arctic Ocean halocline (Aagaard and Carmack, 1989).

4.7. Winds and atmospheric forcing

Ice cover on the eastern Bering Sea shelf is strongly influenced by the direction of winter winds. Winter winds transport Arctic air southwards. Air temperatures typical of Arctic-origin are necessary to cool the surface waters and allow the formation of ice (Stabeno et al., 2007; 2010). Until recently, these winter winds had remained relatively constant (Brown and Arrigo, 2012), allowing the continued formation of winter sea-ice cover in the Bering sea at approximately 465,000 km^2 over the satellite record, in contrast to significant reductions in summer sea ice in the Arctic Ocean. The seasonal Bering Sea ice pack between 1980-2010 showed no sign of reduction (Brown et al., 2011), with warming trends limited to the summer, when the Bering Sea is ice free. Wendler et al. (2014) identified an association between extensive ice extent and decreased atmospheric pressure over mainland Alaska and increased atmospheric pressure in eastern Siberia. These conditions lead to northerly wind vectors for years with heavy ice, which push ice south.

We found that the strength and position of the Aleutian Low differs between warm phases and cold phases in the Bering Sea. The position of the Aleutian Low was relatively constant in warm years. Cold years were characterized by a more variable position of the center of the Aleutian Low system. Similar phenomena have been noted in the Bering-Chukchi circulation field (Rodionov et al., 2007; Overland et al., 1999). Danielson et al. (2014) also noted that mean winter position of the Aleutian Low shifted eastward in 2006-2011 relative to a more westward position in 2000-2005 and in recent warm years.

In the Chukchi Sea, the Aleutian Low position is known to be largely responsible for wind-driven upwelling (Pickart et al., 2009; Pisareva et al., 2019). Our results suggest that it also has important effects on circulation and thermal dynamics in the Bering Sea.

4.8. The distinct nature of the NBS

Results of the DBSCAN cluster analysis confirm past analyses that distinguish the NBS (> 60°N) from other regions of the Bering Sea. Many regional studies that distinguish marine systems also separate the NBS from other parts of the Bering Sea, often including it in the Chukchi Sea large marine ecosystem (e.g. the United National Intergovernmental Oceanographic Commission; Fanning et al., 2015; Chandler and Yoo, In Press). Many of these important distinctions may be less evident absent sea ice.

The 60°N latitude marks the historical minimum southern extent of maximum sea-ice cover in the Bering Sea. Until recently, areas north of this latitude were covered with sea ice every year, while areas south were characterized by variable annual sea-ice extent (Sigler et al., 2010). This had important implications for atmospheric-oceanic interactions, wind mixing, wave activity, salinity, heat content, stratification, and phenology and pathways of primary productivity (planktonic production and ice algal pathways). These observations are supported by historical data 1958-1980 (Overland and Pease, 1982), as well as more recent analyses (Sigler et al., 2014). In terms of physics, there are some distinct dynamics that are likely to permanently distinguish areas north of 60°N. This is the approximate point where the Bering Slope current turns off-shelf to flow westward (Ladd, 2014), flow intensifies along the east coast of Siberia (creating the Anadyr Current, Kinder et al., 1986), and geostrophic velocity vectors and circulation patterns on the shelf diverge (Cokelet et al., 2016; Hollowed et al., 2012). This latitude also features major influx of freshwater inputs via the Yukon and Kuskokwim rivers; distinct patterns in upper-to-lower density differences on the shelf are also pronounced at approximately 60°N (Cokelet et al., 2016). Intensified northward flow occurs in the approach to Bering Strait (Woodgate and Aagaard, 2005) and differences are noted in bottom and surface velocity vectors (Zhang et al., 2012). Other attributes of physical oceanography, however, appear to be in transition. Evident breaks in vertical hydrographic, temperature, and salinity profiles (Goes et al. 2014) and distinct patterns in stratification (Ladd and Stabeno, 2012) are likely to change in the absence of ice. ROMS model results that formerly suggest significant difference in patterns at 60°N for sea surface temperature, ice cover, and wind stress (Hermann et al., 2016) are not apparent in more recent model predictions (Hermann, Pacific Marine Environmental Laboratory, NOAA, Seattle, USA, personal communication).

It is important to monitor how shifts in the physical system might influence the ecology of the systems (Post et al., 2013). Notable differences north and south of 60°N have been noted in phytoplankton community production and trends (Mordy et al. 2012) and in large crustacean zooplankton abundance and species composition (Eisner et al., 2015; Hermann et al., 2016; Siddon et al., In Press). These patterns are also noted in larval fish assemblages (Eisner et al., 2015; Parker-Stetter et al., 2016; Siddon et al., In Press) forage fishes, (Andrews et al., 2016; Baker, 2020), and adult fishes and invertebrate communities (Stevenson and Lauth 2012; Mueter and Litzow, 2008; Baker and Hollowed, 2014; Stevenson and Lauth, 2019). Subsistence harvest and community dynamics are also distinct north and south of 60°N (Renner and Huntington, 2014).

4.9. Implications of reduced sea ice and the erosion of thermal barriers in Bering-Chukchi system

Ice thickness, age, and extent have changed rapidly in recent decades in the Arctic (Cosimo, 2012). Reductions in sea-ice duration and declines in multiyear ice cover are leading to extensive open water in the Central Arctic Ocean, particularly in summer and fall, increasing availability for commercial activity, especially international shipping (Van Pelt et al., 2017). Continued sea-ice loss will ensure the Arctic is increasingly accessible for oil and gas exploration and developments and marine shipping (United States Navy, 2014). Increased expanse of open water also increases fetch and wave action (Thomson and Rogers, 2014). This may break up the ice that is present, changing the character of that ice, with implications for human transport (subsistence activities) and marine mammal use (ice seals, walrus, polar bears). These trends, evident in the broader Arctic should be closely monitored in the Pacific-Arctic gateway.

4.10. Prospects for increased international collaboration and data sharing

Despite several coordinated international efforts, the ability to access and visualize data in a unified data portal is limited. Data sharing is often dependent on personal correspondence between colleagues (Van Pelt et al., 2017). An integrated Arctic Ocean Observing System has emerged to complement regional networks, but none are comprehensive. International science institutions such as PICES and regional networks such as PAG have been instrumental in promoting information standardization and information sharing (Eisner et al., 2017; Baker et al., 2018) and research institutions such as NPRB have been effective in coordinating scientific efforts across diverse institutions and internationally. Further collaboration between national science agencies including NOAA (USA), VNIRO (RUS), Fisheries and Oceans Canada (DFO-CAN), Japan Agency for Marine-Earth Science and Technology (JAMSTEC-JPN), the Korea Institute of Ocean Science and Technology (KIOST-KOR), and the State Oceanic

Administration (SOA-CHN) are promising. Continued efforts to integrate data and perspectives across national boundaries are increasingly necessary.

Acknowledgements

This research was initiated in discussions related to the 2016 and 2017 North Pacific Marine Science Organization (PICES) Annual Science Meeting workshops on data sharing and collaboration in the northern Bering Sea in San Diego and Vladivostok, Russia, convened by M. Baker, K. Kivva and L. Eisner. Analyses were further developed through subsequent discussion and collaboration, related to the development of the PICES North Pacific Ecosystem Status Report in 2018 in Yokohama, Japan. The dedicated efforts of A. Bychkov, H. Batchelder, S. Batten, P. Mundy, P. Chandler, and S. Yoo to coordinate these meetings is also greatly appreciated. We also thank L. Eisner, V. Lobanov, Y. Zuenko, V. Kulik, E. Siddon, E. Farley, F. Mueter, and S. Danielson for their contributions to these discussions. Support provided to these efforts by PICES, NPRB, NOAA, and VNIRO is greatly appreciated. Analyses were also supported by the Ministry of Science and Education of Russia, theme 0149-2019-0004. This research was further informed by the NPRB Arctic Integrated Ecosystem Research Program, which has facilitated and continued US-Russian collaborative research. This work builds on the extensive and continued efforts of the NOAA Alaska Fisheries Science Center and Pacific Marine Environmental Laboratory and we thank P. Stabeno, R. Lauth, A. Hollowed, A. Hermann, and K. Holsman for conversations that informed this analysis. We also thank J. Gann, A. Gray, P. Stabeno, and C. Ladd for review of the manuscript and K. Drinkwater for editing and facilitating the publication. The findings and conclusions are those of the authors and do not necessarily represent those of the associated institutions. This is NPRB publication ArcticIERP-05.

References

Aagaard, K., Carmack, E.C., 1989. The role of sea ice and other fresh water in the Arctic circulation. J. Geophys. Res. Oceans 94, 14485-98.

Amante, C, Eakins, B.W., 2009. Etopo1 1 arc-minute global relief model: Procedures, data sources and analysis. NOAA Technical Memorandum, NESDIS NGDC-24: 1-19.

Andrews, A.G., Strasburger, W.W., Farley, E.V., Murphy, J.M., Coyle, K.O., 2016. Effects of warm and cold climate conditions on capelin (*Mallotus villosus*) and Pacific herring (*Clupea pallasii*) in the eastern Bering Sea. Deep-Sea Res. II 134, 235-46.

Asahara, Y., Takeuchi, F., Nagashima, K., Harada, N., Yamamoto, K., Oguri, K., Tadai, O., 2012. Provenance of terrigenous detritus of the surface sediments in the Bering and Chukchi Seas as derived from Sr and Nd isotopes: Implications for recent climate change in the Arctic regions. Deep-Sea Res. II 61, 155-171.

Aydin, K.Y., Lapko, V.V., Radchenko, V.I., Livingston, P.A., 2002. A comparison of the eastern Bering and western Bering Sea shelf and slope ecosystems through the use of mass-balance food web models. NOAA Technical Memorandum NMFS-AFSC, 130.

Aydin, K., Mueter, F., 2007. The Bering Sea—a dynamic food web perspective. Deep-Sea Res. II 54, 2501-2525.

Baker, M.R, Hollowed, A.B., 2014. Delineating ecological regions in marine systems: Integrating physical structure and community composition to inform spatial management in the eastern Bering Sea. Deep-Sea Res. II 109, 215-40.

Baker, M.R., Kivva, K.K., Eisner, L., 2018. Workshop – The role of the northern Bering Sea in modulating the Arctic II: International interdisciplinary collaboration". PICES Press 26, 15-19; https://search.proquest.com/openview/37716f6583252e708e1825d84c0f2dd0/1?pq-origsite=gscholar&cbl=666306.

Baker, M.R., 2020. Contrast of warm and cold phases in the Bering Sea to understand spatial distributions of Arctic and subarctic gadids. Special Issue: Arctic Gadids in a Changing Climate. Pol. Biol.

Baker, M.R., Farley E.V., Danielson, S.L., Ladd C., Stafford K.M., Dickson, D.M.S., 2020. Understanding ecosystem processes, timing, and change in the Pacific Arctic. Deep-Sea Res. II.

Baker, M.R., In Press. The Northern Bering Sea. North Pacific Ecosystem Status Report. North Pacific Marine Science Organization (PICES). Special Publication. https://meetings.pices.int/projects/npesr

Barbeaux, S.J., Hollowed, A.B., 2018. Ontogeny matters: Climate variability and effects on fish distribution in the eastern Bering Sea. Fish. Oceanogr. 27, 1-15.

Brown, Z.W., Van Dijken, G.L., Arrigo, K.R., 2011. A reassessment of primary production and environmental change in the Bering Sea. J. Geophys. Res-Oceans. 116, C8.

Brown, Z.W., Arrigo, K.R., 2012. Contrasting trends in sea ice and primary production in the Bering Sea and Arctic Ocean. ICES J. Mar. Sci. 69, 1180-93.

Brown, Z.W., Lowry, K.E., Palmer, M.A., van Dijken, G.L., Mills, M.M., Pickart, R.S., Arrigo, K.R., 2015. Characterizing the subsurface chlorophyll a maximum in the Chukchi Sea and Canada Basin. Deep-Sea Res. II 118, 88-104.

Chandler, P., Yoo, S., In Press. North Pacific Ecosystem Status Report. North Pacific Marine Science Organization. PICES, Special Publication.

Chapman, W., Walsh, J., 1993. Recent variations in sea ice and air temperature at high latitudes. BAMS 74, 33-48.

Coachman, L.K., Aagaard, K., 1966. On the water exchange through Bering Strait, Limnol. Oceanogr. 11, 44-59.

Coachman, L.K., 1993. On the flow field in the Chirikov Basin. Cont. Shelf Res. 13, 481–508.

Coachman, L.K., Aagaard, K., Tripp, R.B., 1975. Bering Strait: the regional physical oceanography. University of Washington Press.

Cokelet, E.D., 2016. 3-D water properties and geostrophic circulation on the eastern Bering Sea shelf. Deep-Sea Res. II 134, 65-85.

Comiso, J.C., 2012. Large decadal decline of the arctic multiyear ice cover, J. Clim. 25, 1176–1193.

Crane, K., Ostrovsky, A., 2015. Introduction to the special issue: Russian-American Long-term Census of the Arctic (RUSALCA). Oceanography 28, 18–3, https://doi.org/10.5670/oceanog.2015.54

Danielson, S., Curchitser, E., Hedstrom, K., Weingartner, T., Stabeno, P., 2011. On ocean and sea ice modes of variability in the Bering Sea. J. Geophys. Res. Ocean 116, C12.

Danielson, S.L., Weingartner, T.J., Hedstrom, K.S., Aagaard, K., Woodgate, R., Curchitser, E., Stabeno, P.J., 2014. Coupled wind-forced controls of the Bering–Chukchi shelf circulation and the Bering Strait throughflow: Ekman transport, continental shelf waves, and variations of the Pacific–Arctic sea surface height gradient. Prog. Oceanogr. 125, 40-61.

Di Lorenzo, E., Schneider, N., Cobb, K.M., Franks, P.J.S., Chhak, K., Miller, A.J., McWilliams, J.C., Bograd, S.J., Arango, H., Curchitser, E., Powell, T.M., 2008. North Pacific Gyre Oscillation links ocean climate and ecosystem change. Geophys. Res. Lett. 35, 8. http://www.pmel.noaa.gov/dbo/about

Duffy-Anderson, J.T., Stabeno, P., Andrews III, A.G., Cieciel, K., Deary, A., Farley, E., Fugate, C., Harpold, C., Heintz, R., Kimmel, D. and Kuletz, K., 2019. Responses of the northern Bering Sea and southeastern Bering Sea pelagic ecosystems following record-breaking low winter sea ice. Geophys. Res. Lett. 46, 9833-9842.

Eisner, L.B., Siddon, E.C., Strasburger, W.W., 2015. Spatial and temporal changes in assemblage structure of zooplankton and pelagic fish in the eastern Bering Sea across varying climate conditions. TINRO 181, 141-160.

Eisner, L., Kivva, K. Baker, M., 2017. Workshop 9 – The role of the northern Bering Sea in modulating arctic environments: Towards international interdisciplinary efforts. PICES science in 2016: A note from the Science Board Chairman 25, 23; https://meetings.pices.int/publications/pices-press/volume25/issue1/PPJan2017.pdf#page=23

Ester, M., Kriegel, H.P., Sander, J., Xu, X., 1996. A density-based algorithm for discovering clusters in large spatial databases with noise. In Kdd 96, 226-231.

Fanning, L., Mahon, R., Baldwin, K., Douglas, S., 2015. Transboundary Waters Assessment Programme (TWAP) Assessment of Governance Arrangements for the Ocean, Volume 1: Transboundary Large Marine Ecosystems. IOC-UNESCO, Paris. IOC Technical Series, 119, 80.

Francis, J.A., Hunter, E., 2007. Changes in the fabric of the Arctic's greenhouse blanket. Envir. Res. Lett. 2, 045011.

Francis, J.A., Hunter, E., 2006. New insight into the disappearing Arctic sea ice. Eos, Trans. Am. Geophys. Union 87, 509-11.

Glebova, S., Ustinova, E., Sorokin, Y., 2009. Long-term tendencies of atmospheric processes and thermal regime in Far-Eastern Seas of Russia in the last three decades. TINRO 159, 285-298.

Goes, J.I., do Rosario Gomes, H., Haugen, E.M., McKee, K.T., D'Sa, E.J., Chekalyuk, A.M., Stoecker, D.K., Stabeno, P.J., Saitoh, S.I. and Sambrotto, R.N., 2014. Fluorescence, pigment and microscopic characterization of Bering Sea phytoplankton community structure and photosynthetic competency in the presence of a Cold Pool during summer. Deep-Sea Res. II 109, 84-99.

Golikov, A.N., Dolgolenko, M.A., Maximovich, N.V., Scarlato, O.A., 1990. Theoretical approaches to marine biogeography. Marine ecology progress series. Oldendorf 63, 289-301.

Grebmeier, J.M., McRoy, C.P., Feder, H.M., 1988. Pelagic-benthic coupling on the shelf of the northern Bering and Chukchi seas. Food supply source and benthic biomass. Mar. Ecol. Prog. Ser. 48, 57-67.

Grebmeier, J.M., Cooper, L.W., Feder, H.M., Sirenko, B.I., 2006. Ecosystem dynamics of the Pacific-influenced northern Bering and Chukchi Seas in the Amerasian Arctic. Prog. Oceanogr. 71, 331-61.

Grebmeier, J.M., Bluhm, B.A., Cooper, L.W., Denisenko, S.G., Iken, K., Kędra, M., Serratos, C. 2015. Time-series benthic community composition and biomass and associated environmental characteristics in the Chukchi Sea during the RUSALCA 2004–2012 Prog. Oceanogr. 28, 116-33.

Hermann, A.J., Gibson, G.A., Bond, N.A., Curchitser, E.N., Hedstrom, K., Cheng, W., Wang, M., Cokelet, E.D., Stabeno, P.J., Aydin, K., 2016. Projected future biophysical states of the Bering Sea. Deep-Sea Res. II 134, 30-47.

Hollowed, A.B., Barbeaux, S.J., Cokelet, E.D., Farley, E., Kotwicki, S., Ressler, P.H., Spital, C., Wilson, C.D., 2012. Effects of climate variations on pelagic ocean habitats and their role in structuring forage fish distributions in the Bering Sea. Deep-Sea Res. II 65, 230-250.

Hollowed, A.B., Barange, M., Beamish, R.J., Brander, K., Cochrane, K., Drinkwater, K., Foreman, M.G., Hare, J.A., Holt, J., Ito, S.I. Kim, S., 2013. Projected impacts of climate change on marine fish and fisheries. ICES J. Mar. Sci. 70, 1023-1037.

Hu, A., Meehl, G.A., Otto-Bliesner, B.L., Waelbroeck, C., Han, W., Loutre, M.F., Lambeck, K., Mitrovica, J.X., Rosenbloom, N., 2010. Influence of Bering Strait flow and North Atlantic circulation on glacial sea-level changes. Nat. Geosci. 2, 118.

Huntington H.P., Danielson S.L., Wiese, F.K., Baker, M.R., Boveng, P., Citta, J.J., De Robertis, A., Dickson, D.M.S., Farley, E.V., George, J.C., Iken, K., Kimmel, D.G., Kuletz, K., Ladd, C., Levine, R., Quakenbush, L., Stabeno, P., Stafford, K.M., Stockwell, D., Wilson, C., 2020. Evidence suggests potential transformation of the Pacific Arctic ecosystem is underway. Nat. Clim. Chang. 1-7.

Khen, G.V., Basyuk, E.O., Vanin, N.S. Matveev, V.I., 2013. Hydrography and biological resources in the western Bering Sea. Deep-Sea Res. II 94, 106-120.

Khen G.V., Basyuk E.O., Matveev V.I., 2015. Parameters of the upper mixed layer and thermocline layer and chlorophyll-a in the western deep basin of the Bering Sea in summer and fall of 2002–2013, Izv. TINRO. — 2015. — Vol. 182. — P. 115–131. [In Russian].

Khen, G.V., Zavolokin, A.V., 2015. The change in water circulation and its implication for the distribution and abundance of salmon in the western Bering Sea in the early 21st century. Russ. J. Mar. Biol. 41(7), 528-547.

Kinder, T.H., Chapman, D.C., Whitehead Jr, J.A., 1986. Westward intensification of the mean circulation on the Bering Sea shelf. J. Phys. Ocean. 16, 1217-1229.

Kinnard, C., Zdanowicz, C.M., Fisher, D.A., Isaksson, E., de Vernal, A., Thompson, L.G., 2011. Reconstructed changes in Arctic sea ice over the past 1,450 years. Nature 479, 509.

Kinney, J.C., Maslowski, W., Aksenov, Y., de Cuevas, B., Jakacki, J., Nguyen, A., Osinski, R., Steele, M., Woodgate, R.A., Zhang, J., 2014. On the flow through Bering Strait: A synthesis of model results and observations. In The Pacific Arctic Region Springer, Dordrecht, pp.167-198.

Kivva K.K., 2016. Delineation of ecological regions in the Bering Sea based on oceanographic data. Trudy VNIRO 164, 62-74. [In Russian].

Kivva, K.K., In Press. The Western Bering Sea. North Pacific Ecosystem Status Report. North Pacific Marine Science Organization (PICES). Special Publication.

Ladd, C., Stabeno, P.J., 2012. Stratification on the Eastern Bering Sea shelf revisited. Deep-Sea Res. II 65, 72-83.

Ladd, C., 2014. Seasonal and interannual variability of the Bering Slope Current. Deep-Sea Res. II 109, 5-13.

Lebrun, M., Vancoppenolle, M., Madec, G., Massonnet, F., 2019. Arctic sea-ice-free season projected to extend into autumn. The Cryosphere 13, 79–96.

Levitus, S., Antonov, J.I., Boyer, T.P. and Stephens, C., 2000. Warming of the world ocean. Science 287, 2225-2229.

Lindsay, R.W., Zhang, J., 2005. The thinning of Arctic sea ice, 1988–2003: Have we passed a tipping point? J. Clim. 18, 4879-94.

Lomas, M.W., Stabeno, P.J., 2014. Introduction to the Bering Sea Project: Volume III. Deep-Sea Res. II 109, 1-4.

Luchin, V.A., 2007. Seasonal variability of water temperature in the active layer of the Far Eastern seas, pp. 232-253, In Akulichev V.A. (Ed.), Far Eastern seas of Russia: in 4 books. Book 1. Oceanological studies. Nauka, Moscow, Russia. [In Russian].

Luchin, V., Kruts, A., Sokolov, O., Rostov, V., Rudykh, N., Perunova, T., Zolotukhin, E., Pischalnik, V., Romeiko, L., Hramushin, V. and Shustin, V., 2009. Climatic Atlas of the North Pacific Seas 2009: Bering Sea, Sea of Okhotsk, and Sea of Japan/V. Akulichev, Yu. Volkov, V. Sapozhnikov, S. Levitus (eds): NOAA Atlas NESDIS 67. Wash. DC: US Gov. Printing Office.

Mantua, N.J., Hare, S.R., Zhang, Y., Wallace, J.M., Francis, R.C., 1997. A Pacific interdecadal climate oscillation with impacts on salmon production. Bull. Am. Meteorol. Soc. 78, 1069-1080.

Maslowski, W., Marble, D.C., Walczowski, W., Semtner, A.J., 2001. On large-scale shifts in the Arctic Ocean and sea-ice conditions during 1979– 98. Ann. Glaciol. 33, 545-550.

Meier, W. N., Fetterer F., Savoie, M., Mallory, S., Duerr, R., Stroeve, J., 2017. NOAA/NSIDC Climate Data Record of Passive Microwave Sea Ice Concentration, Version 3. Boulder, Colorado USA. NSIDC: National Snow and Ice Data Center. doi: https://doi.org/10.7265/N59P2ZTG. [10 July 2019].

Meier, W.N., Fetterer, F., Windnagel, A.K., 2017. Near-Real-Time NOAA/NSIDC Climate Data Record of Passive Microwave Sea Ice Concentration, Version 1. https://doi.org/10.7265/N5FF3QJ6. [July 2019].

Mordy, C.W., Cokelet, E.D., Ladd, C., Menzia, F.A., Proctor, P., Stabeno, P.J. Wisegarver, E., 2012. Net community production on the middle shelf of the eastern Bering Sea. Deep-Sea Res. II 65, 110-125.

Mueter, F.J., Litzow, M.A., 2008. Sea ice retreat alters the biogeography of the Bering Sea continental shelf. Ecol. Appl. 18, 309-320.

Mueter, FJ, Weems, J., Farley, E.V., Sigler, M.F., 2017. Arctic ecosystem integrated survey (Arctic Eis): marine ecosystem dynamics in the rapidly changing Pacific Arctic Gateway. Deep-Sea Res. II 135, 1–6, http://dx.doi.org/10.1016/j.dsr2.2016.11.005.

Natarov, V.V., 1963. On the water masses and currents of the Bering Sea [O vodnykh massakh i techeniyakh Beringova moray] (On Water Masses and Currents in the Bering Sea). Trudy VNIRO, 48(1). [In Russian].

Nghiem, S., Rigor, R., Perovich, D., Clemente-Colon, P., Wetherly, J., Neumann, G., 2007. Rapid reduction of Arctic perennial sea ice. JGR Lett. 34, GL031480.

Ogi, M., Yamazaki, K., Wallace, J.M., 2010. Influence of winter and summer surface wind anomalies on summer Arctic sea ice extent. Geophys. Res. Lett. 39, L08502.

Ortiz, I., Aydin, K., Hermann, A.J., Gibson, G.A., Punt, A.E., Wiese, F.K., Eisner, L.B., Ferm, N., Buckley, T.W., Moffitt, E.A. Ianelli, J.N., 2016. Climate to fish: Synthesizing field work, data and models in a 39-year retrospective analysis of seasonal processes on the eastern Bering Sea shelf and slope. Deep-Sea Res. II 134, 390-412.

Overland, J.E., Pease, C.H., 1982. Cyclone climatology of the Bering Sea and its relation to sea ice extent. Monthly Weather Review, 110, 5-13.

Overland, J., Adams, J., Bond, N., 1999. Decadal variability of the Aleutian Low and its relation to high-latitude circulation. J. Clim.12, 1542–1548.

Overland, J., Wang, M., Wood, K., Percival, D., Bond, N., 2012. Recent Bering Sea warm and cold events in a 95-year context. Deep-Sea Res. II 6–13.

Pante, E., Simon-Bouhet, B., 2013. marmap: A Package for Importing, Plotting and Analyzing Bathymetric and Topographic Data in R. PLoS One 8(9): e73051. https://doi.org/10.1371/journal.pone.0073051

Panteleev, G., Yaremchuk, M., Luchin, V., Nechaev, D., Kukuchi, T., 2012. Variability of the Bering Sea circulation in the period 1992-2010. J. Oceanogr. 68, 485-96. DOI 10.1O07/S10872-012-0113-O

Parker-Stetter, S., Urmy, S., Horne, J., Eisner, L., Farley, E., 2016. Factors affecting summer distributions of Bering Sea forage fish species: assessing competing hypotheses. Deep-Sea Res. II 134, 255-269.

Pickart, R.S., Weingartner, T.J., Pratt, L.J., Zimmermann, S., Torres, D.J., 2005. Flow of winter-transformed Pacific water into the Western Arctic. Deep-Sea Res. II 52, 3175-98.

Pickart, R.S., Moore, G.W.K., Torres, D.J., Fratantoni, P.S., Goldsmith, R.A., Yang, J., 2009. Upwelling on the continental slope of the Alaskan Beaufort Sea: storms, ice, and oceanographic response. J. Geophys. Res. Ocean 114, C00A13. https://doi.org/10.1029/2008JC005009.

Pisareva, M.N., 2018. An overview of the recent research on the Chukchi Sea water masses and their circulation. Russ. J. Earth Sci. 18, 4.

Pisareva, M.N., Pickart, R.S., Spall, M.A., Nobre, C., Torres, D.J., Moore, G.W.K., Whitledge, T.E., 2015. Flow of Pacific water in the western Chukchi Sea: Results from the 2009 RUSALCA expedition. Deep-Sea Res. II 105, 53-73.

Pisareva M.N., Pickart, R.S., Lin, P., Fratantoni, P., Weingartner, T.J., 2019. On the nature of wind-forced upwelling in Barrow Canyon. Deep-Sea Res. II 10.1016/j.dsr2.2019.02.002.

Parkinson, C. L., 2014. Spatially mapped reductions in the length of the Arctic sea ice season. Geophys. Res. Lett. 41, 4316–4322.

Pease, C.H., 1980. Eastern Bering Sea ice processes. Mon Weather Rev. 108, 2015-2023.

Peng, G., Steele, M., Bliss, A., Meier, W., Dickinson, S., 2018. Temporal Means and Variability of Arctic Sea Ice Melt and Freeze Season Climate Indicators Using a Satellite Climate Data Record. Remote Sensing 10, 1328.

Perovich, D.K., Light, B., Eicken, H., Jones, K.F., Runciman, K., Nghiem, S.V., 2007. Increasing solar heating of the Arctic Ocean and adjacent seas, 1979-2005: Attribution and the role of the ice-albedo feedback. Geophys. Res. Lett. 34, L19505.

Pickart, R.S., Moore, G.W.K., Mao, C., Bahr, F. Nobre, C., 2016. Circulation of winter water on the Chukchi shelf in early summer, Deep-Sea Res. II, 130, 56–75.

Plotnikov V.V., Vakulskaya N.M., 2012. Variability of ice conditions in the Bering Sea in the second half of 20 century and the beginning of 21 century // Izv. TINRO. Vol. 170. pp.220–228. [In Russian].

Polyakov, I., Alexeev, V.A., Ashik, I.M., Bacon, S., Beszynska-Moller, A., Carmack, E.C., Dmitrenko, I.A., Fortier, L., Gascard, J.C., Hansen, E., Holemann, J., Ivanov, V.V., Kikuchi, T., Kirillov, S., Lenn, Y.D., McLaughlin, F.A., Piechura, J., Repina, I., Timokhov, L.A., Walczoowski, W., Woodgate, R., 2011. Fate of the early 2000's Arctic warm water pulse. Bull. Am. Meteorol. Soc. 92, 561–566.

Post, E., Bhatt, U.S., Bitz, C.M., Brodie, J.F., Fulton, T.L., Hebblewhite, M., Kerby, J., Kutz, S.L., Stirling, I., Walker, D.A., 2013. Ecological consequences of sea ice decline. Science 341, 519–524.

Ratmanov, G.E., 1937. On the hydrology of the Bering and Chukchi seas. Explor. Far-East Seas 5, 10-18.
Renner, M., Huntington, H.P., 2014. Connecting subsistence harvest and marine ecology: a cluster analysis of communities by fishing and hunting patterns. Deep-Sea Res. II 109, 293-299.
Reynolds, R.W., Rayner, N.A., Smith, T.M., Stokes, D.C., Wang, W., 2002. An improved in situ and satellite SST analysis for climate. J. Clim. 15, 1609-1625.
Rigor, I., Wallace, J., 2004. Variation in the age of Arctic sea ice and summer sea ice extent. JGR Letter 31, GL019492
Rigor, I.G., Wallace, J.M., Colony, R.L., 2002. Response of sea ice to the Arctic Oscillation. J. Clim. 15, 2648–2663.
Roach, A.T., Aagaard, K., Pease, C.H., Salo, S.A., Weingartner, T., Pavlov, V., Kulakov M., 1995. Direct measurements of transport and water properties through the Bering Strait. J. Geophys. Res. 100, 18443-18457.
Rodionov, S., Bond, N., Overland, J., 2007. The Aleutian Low. Stormtracks, and winter climate variability in the Bering Sea. Deep-Sea Res. II 54, 2560–2577.
Sample, T.M., Nichol, D.G., 1994. Results of the 1990 US-USSR cooperative bottom trawl survey of the eastern and northwestern Bering Sea continental shelf.
Sander, J., Ester, M., Kriegel, H.P., Xu, X. 1998. Density-based clustering in spatial databases: The algorithm gdbscan and its applications. Data Min. Knowl. Disc. 2, 169-194.
Schubert, E., Sander, J., Ester, M., Kriegel, H.P., Xu, X., 2017. DBSCAN revisited, revisited: why and how you should (still) use DBSCAN. ACM Transactions on Database Systems (TODS) 42, 19.
Serreze, M., Holland, M., Stroeve, J., 2007. Perspectives on the Arctic's shrinking sea-ice cover. Science 315, 1533–1536.
Shimada, K., Kamoshida, T., Itoh, M., Hishino, S., Carmack, E., McLaughlin, F., Zimmerman, S., Proshutinsky, A., 2006. Pacific Ocean inflow: Influence on catastrophic reduction of sea ice cover in the Arctic Ocean. Geophys. Res. Lett. 33, l08605.
Siddon, E., In Press. The Eastern Bering Sea. North Pacific Ecosystem Status Report. North Pacific Marine Science Organization (PICES). Special Publication.
Siddon, E., Zador, S., Aydin, K., 2017 Ecosystem Assessment Ecosystem Status Report 2017. Edited by Siddon E and Zador S. Bering Sea and Aleutian Islands Stock Assessment and Fishery Evaluation report. North Pacific Fishery Management Council. Anchorage, AK.
Siddon E., Stephani Zador, S., 2019. Ecosystem Status Report - Eastern Bering Sea. NPFMC Bering Sea and Aleutian Islands SAFE Report. https://access.afsc.noaa.gov/REFM/REEM/ecoweb/pdf/2019EBSecosys.pdf
Sigler, M.F., Harvey, H.R., Ashjian, C.J., Lomas, M.W., Napp, J.M., Stabeno, P.J., Van Pelt, T.I., 2010. How does Climate change affect the Bering Sea ecosystem? Trans. Am. Geophys. Union 91, 457-458.
Sigler, M.F., Stabeno, P.J., Eisner, L.B., Napp, J.M., Mueter, F.J., 2014. Spring and fall phytoplankton blooms in a productive subarctic ecosystem, the eastern Bering Sea, 1995–2011. Deep-Sea Res. II 109, 71-83.
Sigler, M.F., Mueter, F.J., Bluhm, B.A., Busby, M.S., Cokelet, E.D., Danielson, S.L., De Robertis, A., Eisner, L.B., Farley, E.V., Iken, K., Kuletz, K.J., 2017. Late summer zoogeography of the northern Bering and Chukchi seas. Deep-Sea Res. II 135, 168-189.
Smith, M.A., Sullender, B.K., Koeppen, W.C., Kuletz, K.J., Renner, H.M., Poe, A.J., 2019. An assessment of climate change vulnerability for Important Bird Areas in the Bering Sea and Aleutian Arc. PloS One 14, 4.
Stabeno, P.J., Bond, N.A., Kachel, N.B., Salo, S.A., Schumacher, J.D., 2001. On the temporal variability of the physical environment over the south-eastern Bering Sea. Fish. Oceanogr. 10, 81–98
Stabeno, P.J., Bond, N.A., Salo, S.A., 2007. On the recent warming of the southeastern Bering Sea Shelf. Deep-Sea Res. II 54, 2599–2618. https://doi.org/10.1016/j.dsr2.2007.08.023
Stabeno, P.J., Kachel, N.B., Moore, S.E., Napp, J.M., Sigler, M., Yamaguchi, A., Zerbini, A.N., 2012a. Comparison of warm and cold years on the southeastern Bering Sea shelf and some implications for the ecosystem. Deep-Sea Res. II 65–70, 31–45. https://doi.org/10.1016/j.dsr2.2012.02.019
Stabeno, P.J., Farley, E.V., Kachel, N.B., Moore, S., Mordy, C.W., Napp, J.M., Overland, J.E., Pinchuk, A.I., Sigler, M.F., 2012b. A comparison of the physics of the northern and southern shelves of the eastern Bering Sea and some implications for the ecosystem. Deep-Sea Res. II 65–70,14–30.

Stabeno, P.J., Danielson, S.L., Kachel, D.G., Kachel, N.B., Mordy, C.W., 2016. Currents and transport on the eastern Bering Sea shelf: An integration of over 20 years of data. Deep-Sea Res. II 134, 13-29.
Stabeno, P.J., Duffy-Anderson, J.T., Eisner, L.B., Farley, E.V., Heintz, R.A., Mordy, C.W., 2017. Return of warm conditions in the southeastern Bering Sea: Physics to fluorescence. PLoS One 12, e0185464. https://doi.org/10.1371/journal.pone.0185464
Stabeno, P.J., Bell, S.W., Bond, N A., Kimmel, D.G., Mordy, C.W., Sullivan, M.E., 2019. Distributed Biological Observatory Region 1: Physics, chemistry and plankton in the northern Bering Sea. Deep-Sea Res. II 162, 8-21. https://doi.org/10.1016/j.dsr2.2018.11.006
Stabeno, P.J., Bell, S.W., 2019. Extreme Conditions in the Bering Sea (2017–2018): Record-Breaking Low Sea-Ice Extent. Geophys. Res. Lett. 46, 8952-8959.
Stevenson, D.E., Lauth, R.R., 2012. Latitudinal trends and temporal shifts in the catch composition of bottom trawls conducted on the eastern Bering Sea shelf. Deep-Sea Res. II 65, 251–259. https://doi.org/10.1016/j.dsr2.2012.02.021
Stevenson, D.E., Lauth, R.R., 2019. Bottom trawl surveys in the northern Bering Sea indicate recent shifts in the distribution of marine species. Pol. Biol. 42, 407-21.
Steele, M., Ermold, W., Zhang, J., 2008. Arctic Ocean surface warming trends over the past 100 years, Geophys. Res. Lett. 35, L02614, doi:10.1029/2007GL031651.
Stroeve, J., Holland, M.M., Meier, W., Scambos, T., Serreze, M. 2007. Arctic sea ice decline: Faster than forecast. Geophys. Res. Lett. 34, 9.
Stroeve, J.C., Crawford, A.D., Stammerjohn, S., 2016. Using timing of ice retreat to predict timing of fall freeze-up in the Arctic. Geophys. Res. Lett. 43, 6332-6340.
SWIPA. 2011. Snow, Water, Ice and Permafrost in the Arctic. Cambridge: Cambridge University Press Executive Summary. Oslo: Arctic Monitoring and Assessment Program, 16 pp.
SWIPA. 2012. Snow, Water, Ice and Permafrost in the Arctic. Cambridge: Cambridge University Press Executive Summary. Oslo: Arctic Monitoring and Assessment Program, 16 pp.
Teng, H., Washington, W.M., Meehl, G.A., Buja, L.E., Strand, G.W., 2006. Twenty-first century Arctic climate change in the CCSM3 IPCC scenario simulations. Climate Dynamics 26, 601-616.
Thomson, J., Rogers, W.E., 2014. Swell and sea in the emerging Arctic Ocean. Geophys. Res. Lett. 41, 3136-3140.
Thorson, J.T., 2019. Measuring the impact of oceanographic indices on species distribution shifts: the spatially varying effect of cold-pool extent in the eastern Bering Sea. Limnol. Oceanogr. 64, 2632-2645.
Torres-Valdés, S., Tsubouchi, T., Bacon, S., Naveira-Garabato, A.C., Sanders, R., McLaughlin, F.A., Whitledge, T. E., 2013. Export of nutrients from the Arctic Ocean. J. Geophys. Res. 118, 1625-1644.
United States Navy, 2014. The United States Navy Artic Roadmap for 2014 to 2030, 38 pp., Department of the Navy, Washington, D.C. [Available at www.navy.mil/docs/USN_arctic_roadmap.pdf.]
Van Pelt, T.I., Huntington, H.P., Romanenko, O.V., Mueter, F.J., 2017. The Missing Middle: Central Arctic Oean gaps in fishery research and science communication. Mar. Pol. 85, 79-86.
Van Pelt, T.I., editor. The Bering Sea Project: Understanding ecosystem processes in the Bering Sea. Anchorage, AK: North Pacific Research Board, 2015.
Verkhunov, A.V., Tkachenko, Y.Y., 1992. Recent observations of variability in the western Bering Sea current system. J. Geophys. Res. Ocean 97, 14369-14376.
Verkhunov, A.V., 1995. The role of hydrological and hydrochemical processes in the formation of bioproductivity of the Bering Sea shelf // In: Complex studies of the Bering Sea ecosystem, Eds.: B.N. Kotenev, V.V. Sapozhnikov. Moscow, VNIRO. p. 52-78. [In Russian].
Walsh, J.J., Dieterle, D.A., Muller-Karger, F.E., Aagaard, K., Roach, A.T., Whitledge, T.E., Stockwell, D., 1997. CO2 cycling in the coastal ocean. II. Seasonal organic loading of the Arctic Ocean from source waters in the Bering Sea. Cont. Shelf Res. 17, 1-3
Walsh, J.J., Dieterle, D.A., Maslowski, W., Grebmeier, J.M., Whitledge, T.E., Flint, M., Sukhanova, I.N., Bates, N., Cota, G.F., Stockwell, D. Moran, S.B., 2005. A numerical model of seasonal primary production within the Chukchi/Beaufort Seas. Deep-Sea Res. II 52, 3541-3576.
Walsh, J.E., Fetterer, F., Scott, S,J., Chapman, W.L., 2017. A database for depicting Arctic sea ice variations back to 1850. Geograph. Rev. 107, 89-107.
Walsh, J., Chapman, W., 1990. Short-term climatic variability of the Arctic. J Climate 3, 237–250.
Watson, J.T., 2019. Spatial and temporal visualizations of satellite-derived sea surface temperatures for Alaska fishery management areas. Pacific States E-journal of Scientific Visualizations (PSESV), Article 003. doi: 10.28966/PSESV.2019.003.

Wendler, G., Chen, L., Moore, B., 2014. Recent sea ice increase and temperature decrease in the Bering Sea area, Alaska. Theor. Appl. Climatol. 117, 393–398

Wang, M., Overland, J.E., 2009. A sea ice free summer Arctic within 30 years? Geophys. Res. Lett. 36, 7.

Wang, J., Cota, G.F., Comiso, J.C., 2005. Phytoplankton in the Beaufort and Chukchi Seas: distribution, dynamics, and environmental forcing. Deep-Sea Res. II 24, 3355-3368.

Whitehouse, G.A., Aydin, K., Essington, T.E., Hunt, G.L., 2014. A trophic mass balance model of the eastern Chukchi Sea with comparisons to other high-latitude systems. Pol. Biol. 37, 911-939.

Wood, K.R., Bond, N.A., Danielson, S.L., Overland, J.E., Salo, S.A., Stabeno, P.J., Whitefield, J., 2015. A decade of environmental change in the Pacific Arctic region. Prog. Oceanogr. 136,12-31.

Woodgate, R.A., Aagaard, K. 2005. Revising the Bering Strait freshwater flux into the Arctic Ocean. Geophys. Res. Lett. 32,2.

Woodgate, R.A., Aagaard, K., Weingartner, T.J., 2005. Monthly temperature, salinity, and transport variability of the Bering Strait through flow. Geophys. Res. Lett. 32, 4.

Woodgate, R.A., Weingartner, T., Lindsay, R., 2007. The 2007 Bering Strait oceanic heat flux and anomalous Arctic sea-ice retreat. Geophys. Res. Lett. 37, 0094-8276.

Woodgate, R.A., Weingartner, T., Lindsay, R., 2010. The 2007 Bering Strait oceanic heat flux and anomalous Arctic sea-ice retreat. Geophys. Res. Lett. 37, 1. https://doi.org/10.1029/2009GL041621.

Woodgate, R.A., Weingartner, T.J., Lindsay, R., 2012. Observed increases in Bering Strait oceanic fluxes from the Pacific to the Arctic from 2001 to 2011 and their impacts on the Arctic Ocean water column. Geophys. Res. Lett. 39, 24.

Woodgate, R.A., Stafford, K.M., Prahl, F.G., 2015. A synthesis of year-round interdisciplinary mooring measurements in the Bering Strait (1990–2014) and RUSALCA (2004–2011). Oceanography 28, 46-67.

Woodgate, R.A., 2018. Increases in the Pacific inflow to the Arctic from 1990 to 2015, and insights into seasonal trends and driving mechanisms from year-round Bering Strait mooring data. Prog. Oceanogr. 160, 124-154.

Wyllie-Echeverria, T., 1995. Seasonal sea ice, the cold pool and gadid distribution on the Bering Sea shelf (Doctoral dissertation).

Wyllie-Echeverria, T.I.N.A. Wooster, W.S., 1998. Year-to-year variations in Bering Sea ice cover and some consequences for fish distributions. Fish. Oceanogr. 7, 159-170.

Zhang, J., Lindsay, R., Schweiger, A., Steele, M., 2013. The impact of an intense summer cyclone on 2012 Arctic sea ice retreat. Geophys. Res. Lett. 40, 720-726.

Zhang, J., Ashjian, C., Campbell, R., Spitz, Y.H., Steele, M., Hill, V., 2015. The influence of sea ice and snow cover and nutrient availability on the formation of massive under-ice phytoplankton blooms in the Chukchi Sea. Deep-Sea Res. II 118, 122-35.

Tables

Table 1. Sea Ice Extent and Sea Ice Area

Bering Sea (March 15)

Time Interval	Extent, Mean ± SD (km^2)	Area, Mean ± SD (km^2)
1979-1999	753,786 ± 103,689	298,719 ± 89,944
2000-2005	648,574 ± 52,652	372,470 ± 41,362
2006-2013	850,977 ± 149,819	201.389 ± 134,204
2014-2016	641,753 ± 80,119	402,340 ± 54,478
2017-2019	402,637 ± 191,671	568,946 ± 153,904

Chukchi Sea (May 15)

Time Interval	Extent, Mean ± SD (km^2)	Area, Mean ± SD (km^2)
1979-1999	823,708 ± 9,095	771,239 ± 23,819
2000-2005	813,072 ± 15,336	746,736 ± 38,737
2006-2013	816,247 ± 8,123	758,523 ± 16,303
2014-2016	798,425 ± 3,908	703,902 ± 4,739
2017-2019	734,284 ± 24,341	625,182 ± 55,788

Notes: Values for sea-ice extent describe the edges of the sea ice and is inclusive of all area within that expanse. Sea-ice extent therefore encompassed all portions of a region determined to be ice-covered, based on a threshold of 15%. If a data cell had greater than 15% ice concentration, the cell was considered ice covered; less than that was determined to be ice-free. Values for sea-ice area reflect the portion of area within that extent that is truly ice covered, accounting for gaps. Sea-ice area values were determined as a function of the percentage of sea ice within each data cells, summed across the full extent to report how much of the total area is covered by ice.

Data Source: National Snow and Ice Data Center, Sea Ice Regional Monthly Index, version 3.0.

Table 2. Cold Pool Extent

Time Interval	1982-1999	2000-2005	2006-2013	2014-2016	2017	2018
Cold Pool Proportional Area	40% ± 30	25% ± 20	58% ± 2	24% ± 4	35%	1.4%

Notes: Total areal coverage of the cold pool as a proportion of the standard EBS survey area.

Figures

Fig. 1. Map of the Pacific Arctic (50-75N, 160E-150W), including the Bering Sea and Chukchi Sea. Important regional areas and broadscale circulation patterns are detailed. Solid arrows indicate observed currents and dashed arrows indicate modeled or quasi-permanent flow; circulation patterns and current vectors in the Chukchi Sea were informed by Pisareva et al. 2015 and Pickart et al. 2016.

Fig. 2a. Annual mean SSTA clusters for regional delineation according to various input parameters in the DBSCAN analysis. The threshold for the number of neighbors (minPts) was set to 31. Radius ε (eps) varied between 0.12 (left), 0.10 (middle), and 0.08 (right).

Fig. 2b. Regions delineated via DBSCAN (final analysis): Region 1 – Chukchi and East Siberian Seas (CS-EES, dark blue), Region 2 – western Bering Sea (WBS, green), Region 3 – eastern Bering Sea (EBS, pink), Region 4 – northern Bering Sea (NBS, orange). Note regions 1-3 are based on clustering of annual mean SSTA values with DBSCAN algorithm. Region 4 is the remaining grid nodes of this region assigned as 'noise' in the DBSCAN analysis. When eps=0.10 is chosen (not eps=0.08 or less) the dark blue region clearly includes large part of the East Siberian sea.

Fig. 3. Sea surface temperature anomalies (SSTA). Trends correspond to the 4 regions defined through cluster analyses (Fig. 2b), including (top plot to bottom plot) CS-ESS (region 1), WBS (region 2), EBS (region 3), and NBS (region 4). The solid black line depicts the monthly regional mean SSTA. Grey semi-transparent shading illustrates the monthly regional standard deviation (i.e., the measure of monthly spatial variability of SSTA in each region). Bars represent annual region mean SSTA. Cold periods relative to the time series mean are shown in blue and warm periods in red. Dots denote months with absolute SSTA values > 1 standard deviation of the monthly regional mean (12 values different for every month); larger dots denote absolute SSTA values > 2 standard deviations. Dots are color-coded according to seasons (winter – JFM, spring – AMJ, summer – JAS, autumn – OND) [data=OISST].

Fig. 4. Top panel: Sea surface temperature (decomposed trend or time series adjusted to remove seasonality) in the EBS (black solid line), WBS (gray dashed line), and NBS (black dashed line). Bottom panel: difference between EBS and NBS sea surface temperatures (dashed line; positive values indicate greater temperatures in the EBS) and time series trend (solid line; seasonality removed). Horizontal lines are the mean temperatures during each of the respective stanzas [data: NOAA Coral Reef Watch version 3.1 operational global satellite daily sea surface temperature 5km resolution].

Fig. 5. Mean sea-ice extent on March 15, compiled in discrete temperature phases: 1980-1999 (high interannual variability), 2000-2005 (warm), 2006-2013 (cold), 2014-2016 (warm), and 2017 and 2018 (anomalously warm). Annual maps for all individual years are available in supplementary materials (Appendix Fig. A-7).

Fig. 6. Mean date of sea-ice retreat, compiled in discrete temperature phases: 1980-1999 (high interannual variability), 2000-2005 (warm), 2006-2013 (cold), 2014-2016 (warm), and 2017 and 2018 (anomalously warm). Annual maps for all individual years are available in supplementary materials (Appendix Fig. A-9).

Fig. 7. Seasonal progression of sea-ice extent (millions of km^2) in the Bering Sea and Chukchi Sea (January-December 1982-2018). Time intervals for warm (2000-2005 and 2014-2016, —) and cold periods (2006-2012, —) and 2017 (- - -) and 2018 (- • -) are contrasted against all other years (1980-1999, —). Inset plot display 2017 (- - -) and 2018 (- • -) contrasted against the 1980-2016 mean (—) and standard deviation (gray area plot).

Fig. 8. Annual extent of open water in the Bering Sea on March 15 (top plot). Annual extent of open water in the Chukchi Sea, May 15 (bottom plot). In the Chukchi Sea, values represent the absolute area of open water within the LME. In the Bering Sea, values are relative to the area of Bering Sea ice extent in 2012, the year of maximal ice extent in the timeseries.

Fig. 9. Boxplots of annual areal extent of open water in the Bering Sea (March 15) and the Chukchi Sea (May 15) for the intervals of analyses, 1982-1999 (high interannual variability), 2000-2005 (warm), 2006-2012 (cold), 2014-2016 (warm), 2017-2018 (anomalously warm). The box represents the interquartile range (middle 50%) of the data, the whiskers contain 90% of the data. Horizontal lines within each box display the median value. Points indicate outliers.

Fig. 10. Areal extent of the Bering Sea cold pool in mid-summer, calculated via bottom temperatures sampled in the NOAA bottom trawl survey. Images 1982-2016 display the area surveyed in the EBS survey grid. Images for 2017 and 2018 show an enlarged sample area that reflects increased survey coverage in those years that included the both the full EBS survey area and also the NBS survey area. Gray lines within the shelf denote the 50 m and 100 m isobaths. The cold pool typically concentrates in the middle shelf, depths 50-100 m. [data: NOAA Alaska Fisheries Science Center, Resource Assessment and Conservation Engineering Division, Groundfish Assessment Program].

Fig. 11. Maps of mean sea level pressure (hPa, color) and 10-m winds (m/s, vectors) for winter months (Nov-Mar) in the Pacific Arctic region [data: ERA5 reanalysis - 1979-2018].

Fig. 12. Maps of mean sea level pressure (hPa, color) and 10-m winds (m/s, vectors) anomalies from climatology (1979-2018) for winter months (Nov-Mar) in the Pacific Arctic region [data: ERA5 reanalysis - 1979-2018].

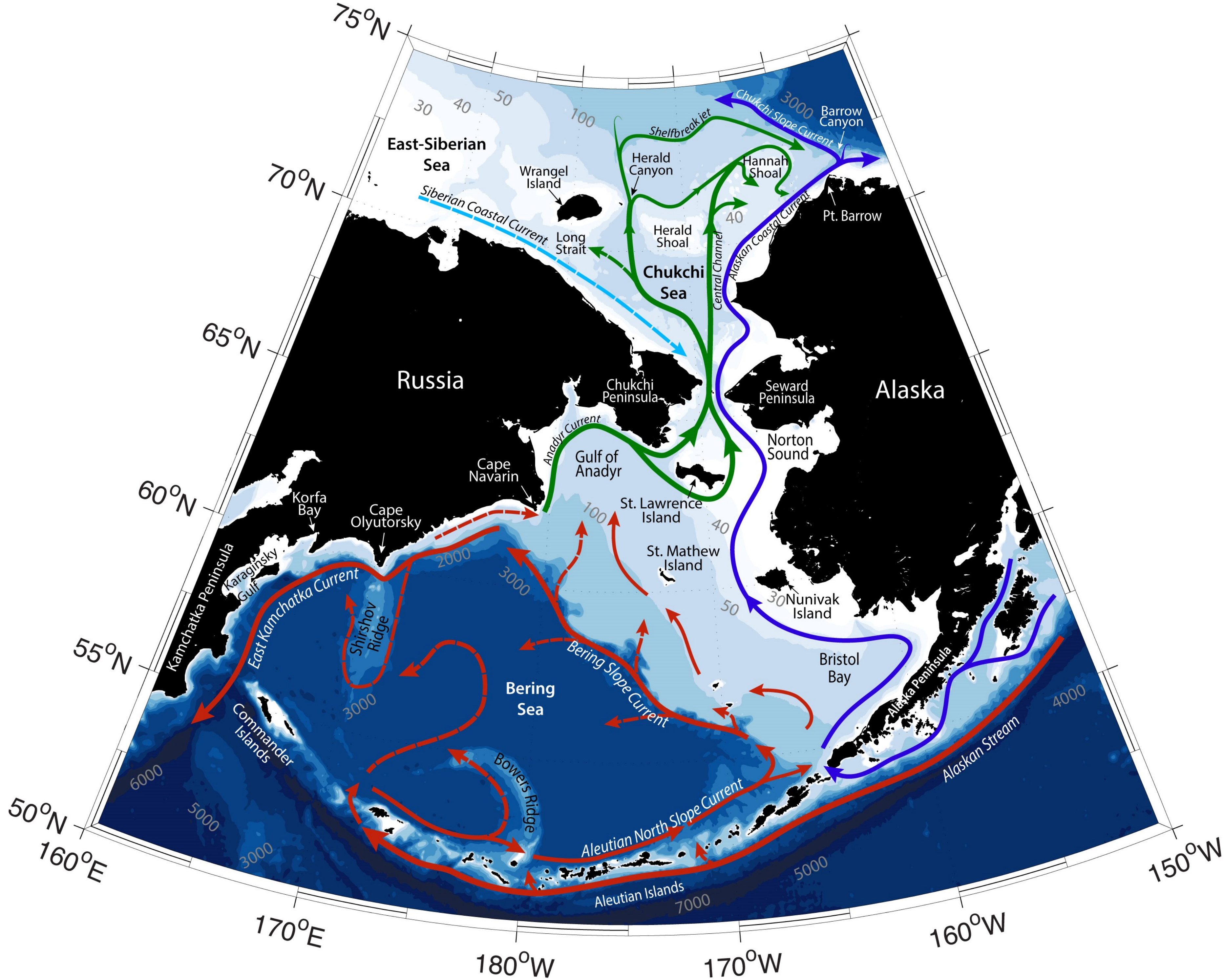
75°N
70°N
65°N
60°N
55°N
50°N
160°E
170°E
180°W
170°W
160°W
150°W
East-Siberian Sea
Wrangel Island
Siberian Coastal Current
Long Strait
Herald Canyon
Shelfbreak jet
Chukchi Slope Current
Barrow Canyon
Hannah Shoal
Pt. Barrow
Herald Shoal
Chukchi Sea
Central Channel
Alaskan Coastal Current
Russia
Alaska
Chukchi Peninsula
Seward Peninsula
Anadyr Current
Gulf of Anadyr
Norton Sound
Cape Navarin
St. Lawrence Island
Korfa Bay
Cape Olyutorsky
Karaginsky Gulf
Kamchatka Peninsula
East Kamchatka Current
Shirshov Ridge
St. Mathew Island
Nunivak Island
Bering Slope Current
Bristol Bay
Bering Sea
Alaska Peninsula
Commander Islands
Bowers Ridge
Alaskan Stream
Aleutian North Slope Current
Aleutian Islands
30
40
50
100
3000
2000
6000
5000
7000
4000

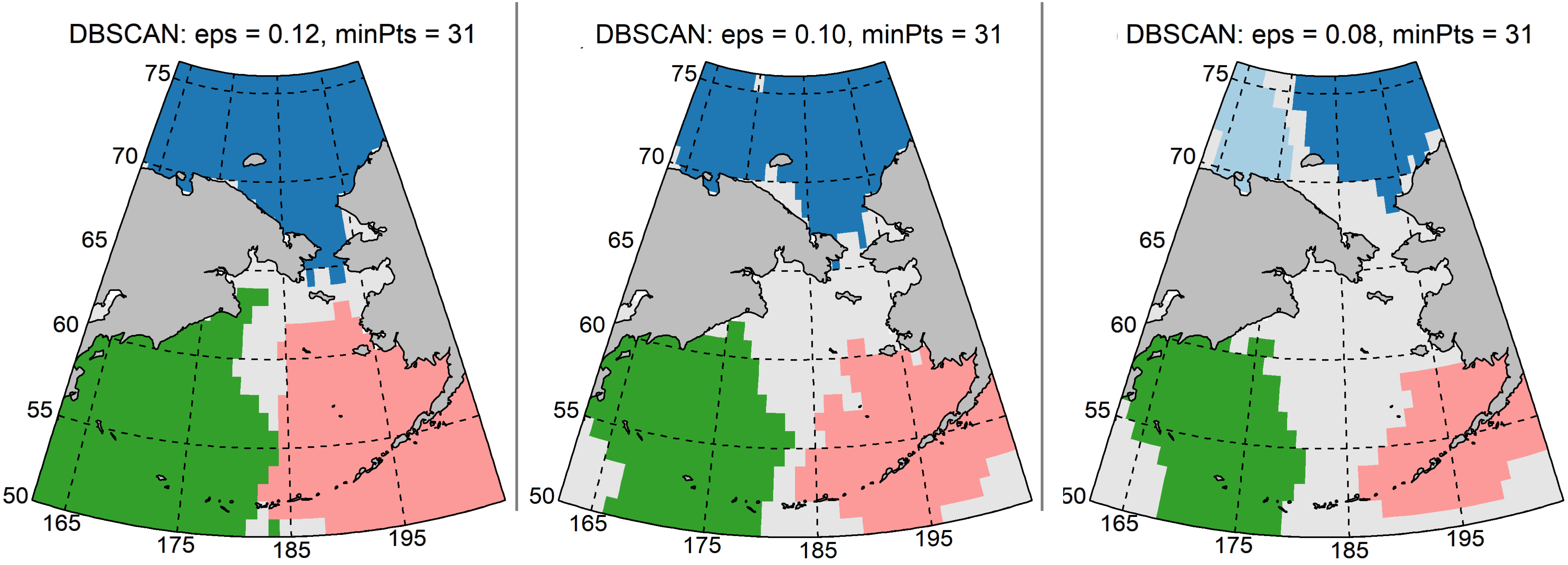
DBSCAN: eps = 0.12, minPts = 31
DBSCAN: eps = 0.10, minPts = 31
DBSCAN: eps = 0.08, minPts = 31
75
70
65
60
55
50
165
175
185
195

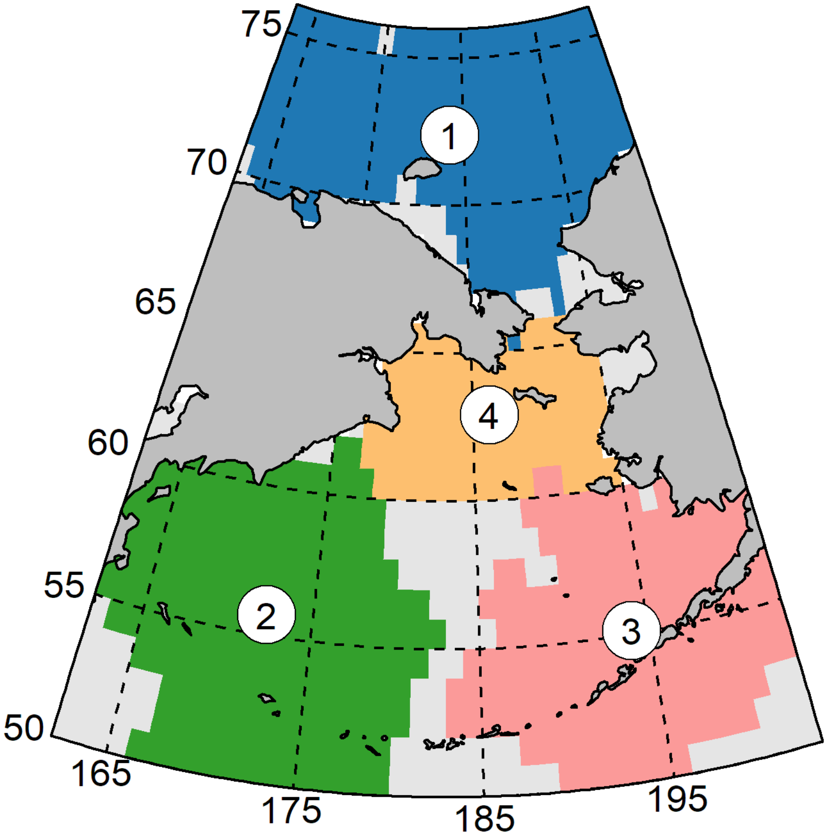
75
70
65
60
55
50
165
175
185
195
1
2
3
4

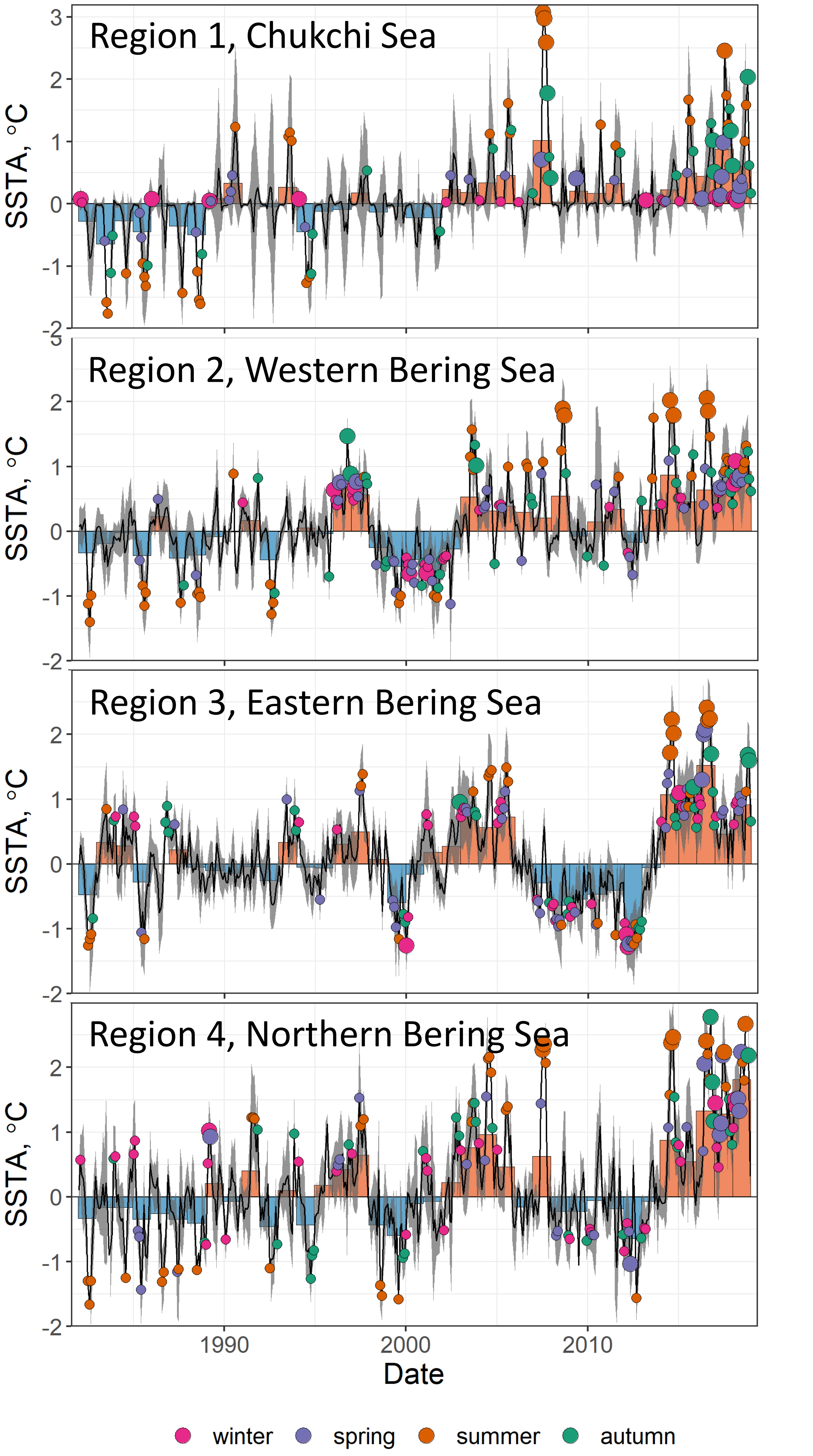

Region 1, Chukchi Sea
Region 2, Western Bering Sea
Region 3, Eastern Bering Sea
Region 4, Northern Bering Sea
SSTA, °C
3
2
1
0
-1
-2
1990
2000
2010
Date
winter
spring
summer
autumn

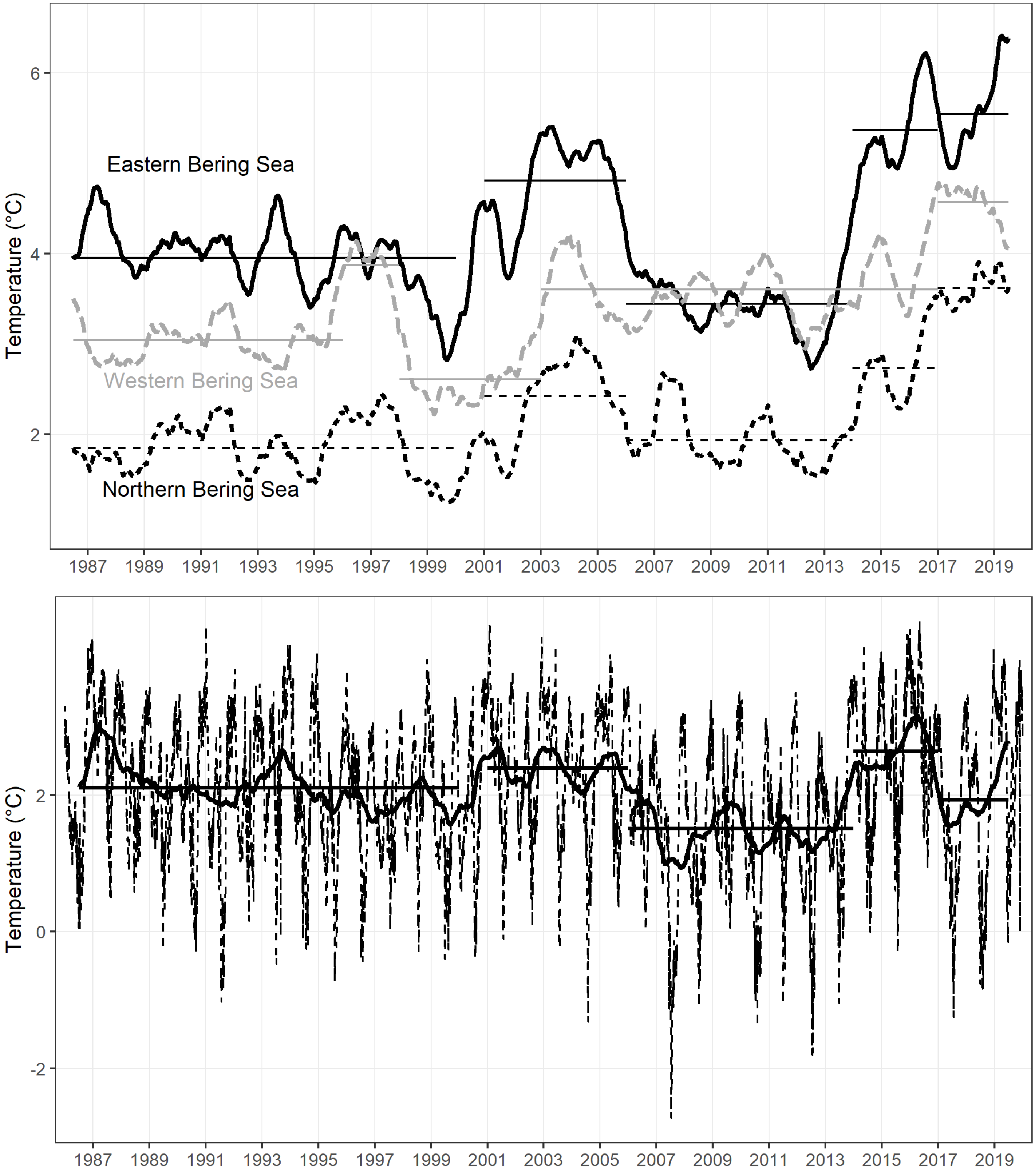
Eastern Bering Sea
Western Bering Sea
Northern Bering Sea
Temperature (°C)
6
4
2
1987 1989 1991 1993 1995 1997 1999 2001 2003 2005 2007 2009 2011 2013 2015 2017 2019
Temperature (°C)
2
0
-2
1987 1989 1991 1993 1995 1997 1999 2001 2003 2005 2007 2009 2011 2013 2015 2017 2019

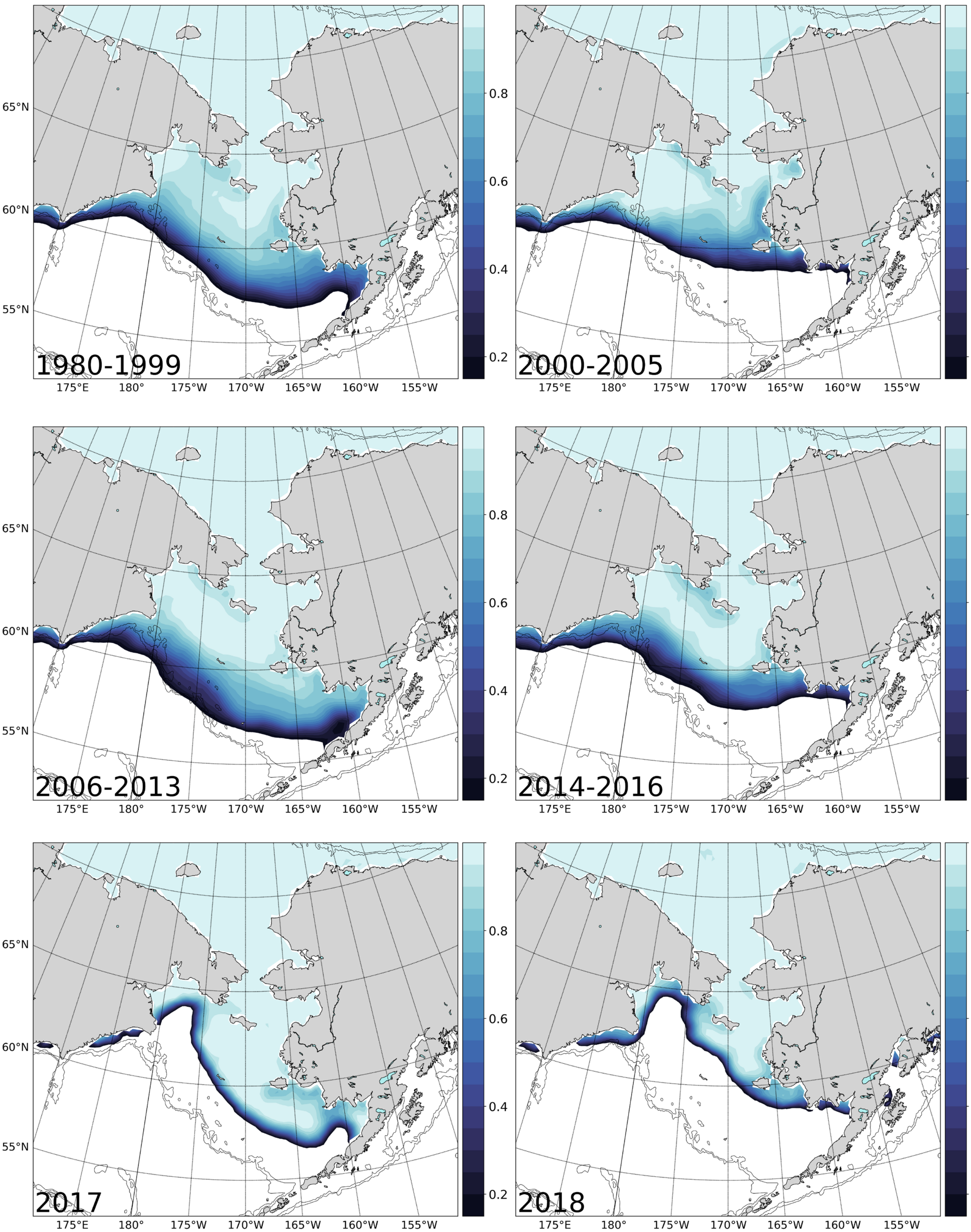
1980-1999
2000-2005
2006-2013
2014-2016
2017
2018
65°N
60°N
55°N
175°E
180°
175°W
170°W
165°W
160°W
155°W
0.8
0.6
0.4
0.2

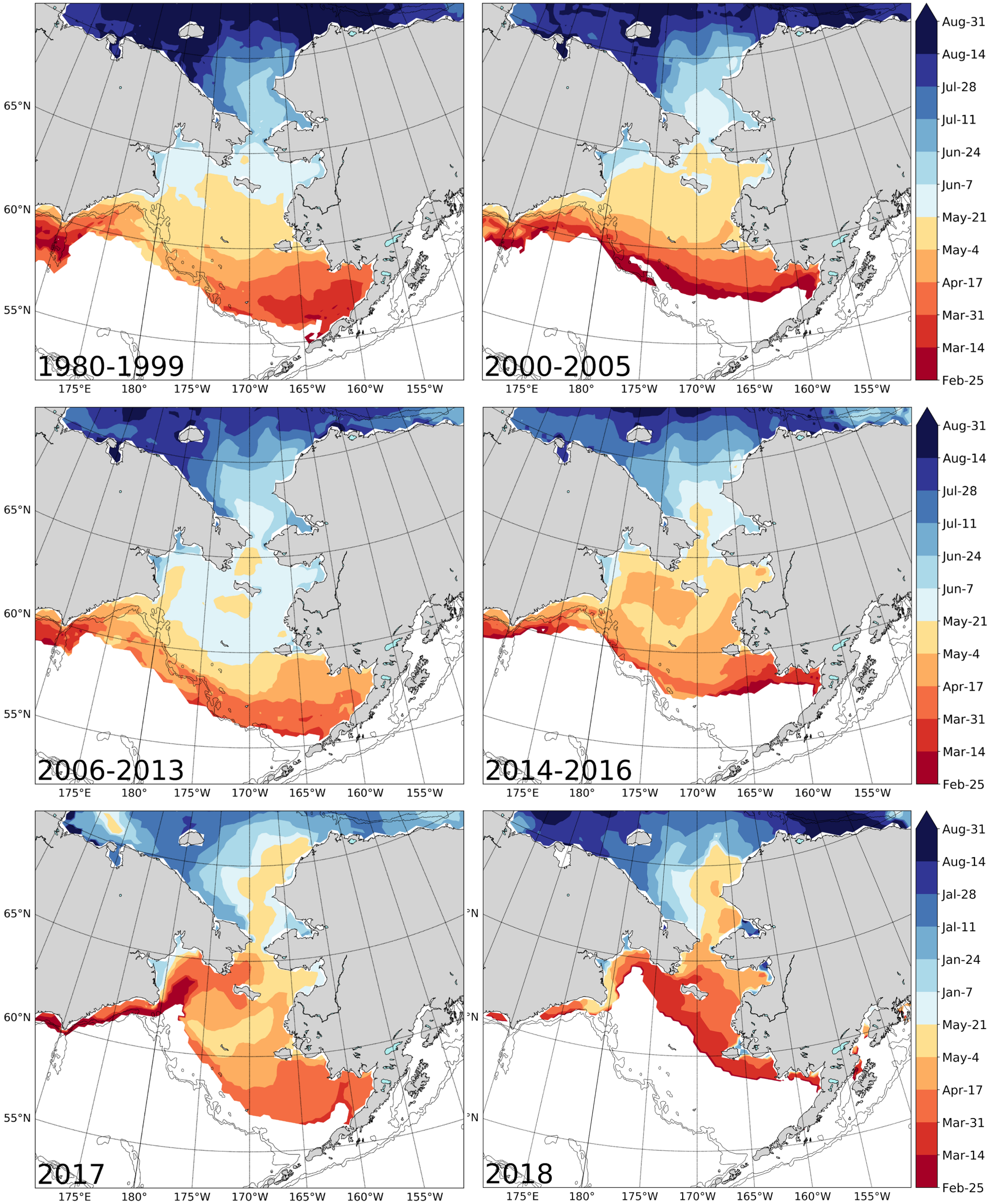

1980-1999
2000-2005
2006-2013
2014-2016
2017
2018
65°N
60°N
55°N
175°E
180°
175°W
170°W
165°W
160°W
155°W
Aug-31
Aug-14
Jul-28
Jul-11
Jun-24
Jun-7
May-21
May-4
Apr-17
Mar-31
Mar-14
Feb-25
Jal-28
Jal-11
Jan-24
Jan-7

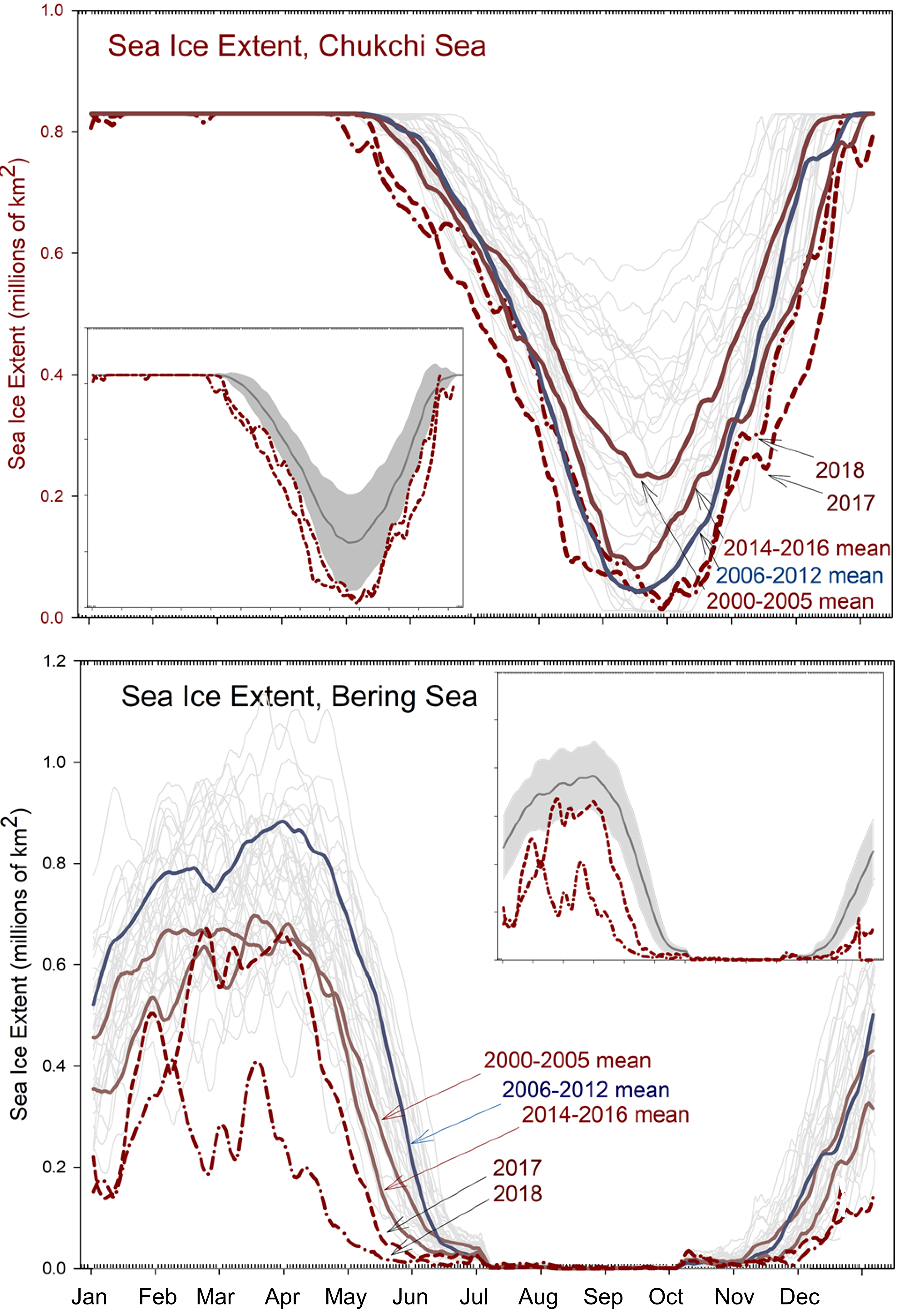

Sea Ice Extent, Chukchi Sea
Sea Ice Extent (millions of km²)
1.0
0.8
0.6
0.4
0.2
0.0
2018
2017
2014-2016 mean
2006-2012 mean
2000-2005 mean
Sea Ice Extent, Bering Sea
Sea Ice Extent (millions of km²)
1.2
1.0
0.8
0.6
0.4
0.2
0.0
2000-2005 mean
2006-2012 mean
2014-2016 mean
2017
2018
Jan
Feb
Mar
Apr
May
Jun
Jul
Aug
Sep
Oct
Nov
Dec

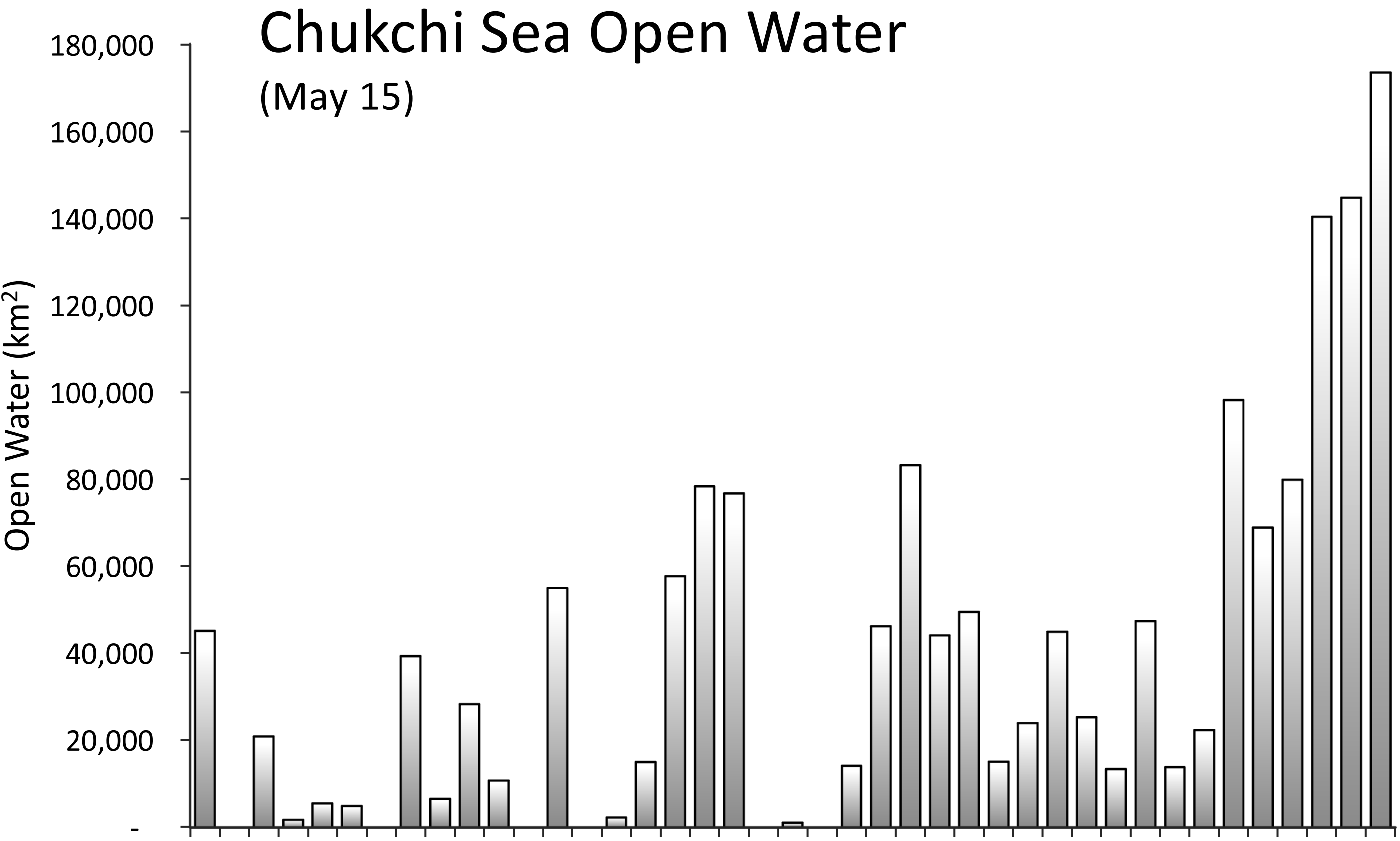
Chukchi Sea Open Water
(May 15)
Open Water (km2)
180,000
160,000
140,000
120,000
100,000
80,000
60,000
40,000
20,000
-

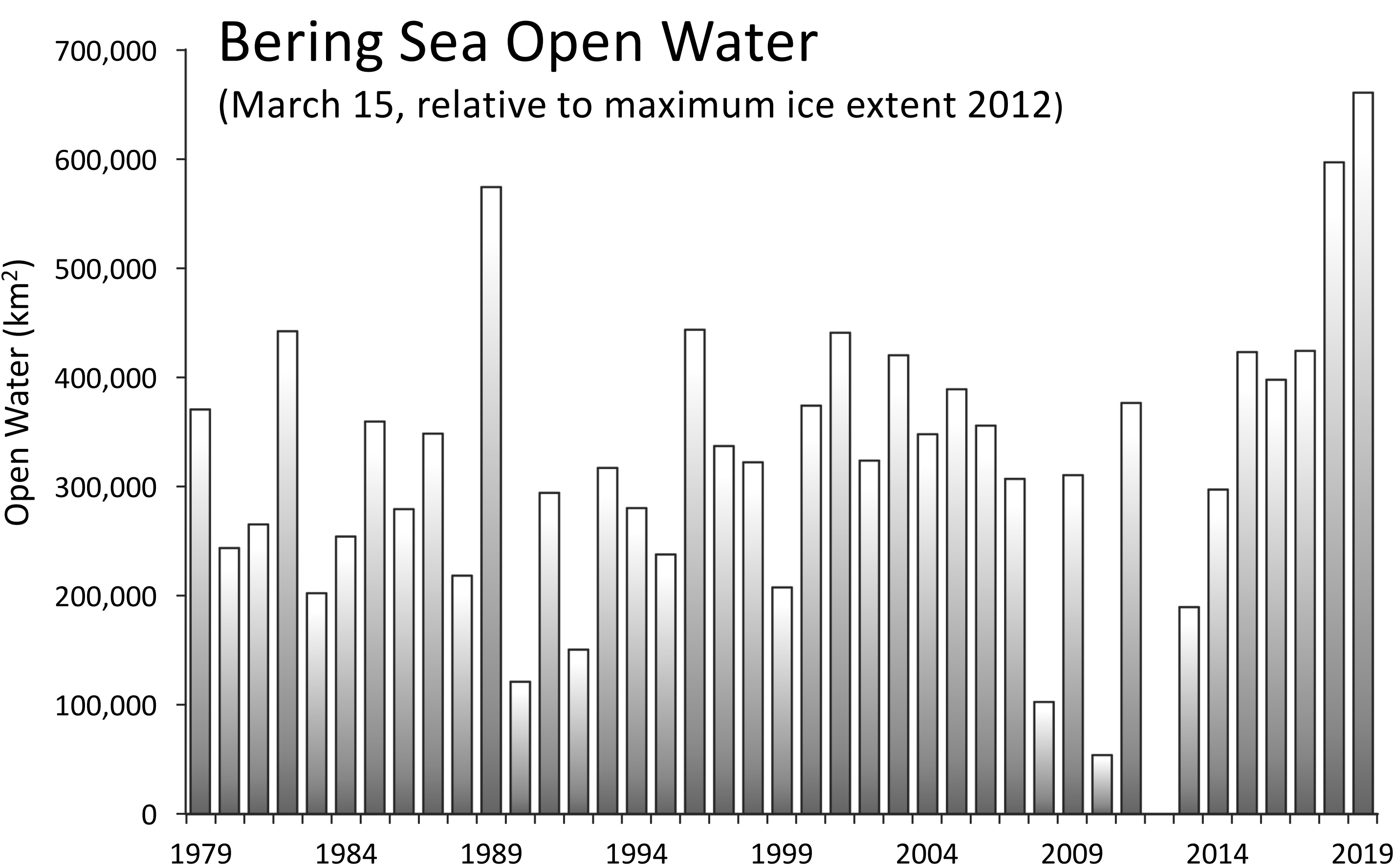
Bering Sea Open Water
(March 15, relative to maximum ice extent 2012)
Open Water (km2)
700,000
600,000
500,000
400,000
300,000
200,000
100,000
0
1979
1984
1989
1994
1999
2004
2009
2014
2019

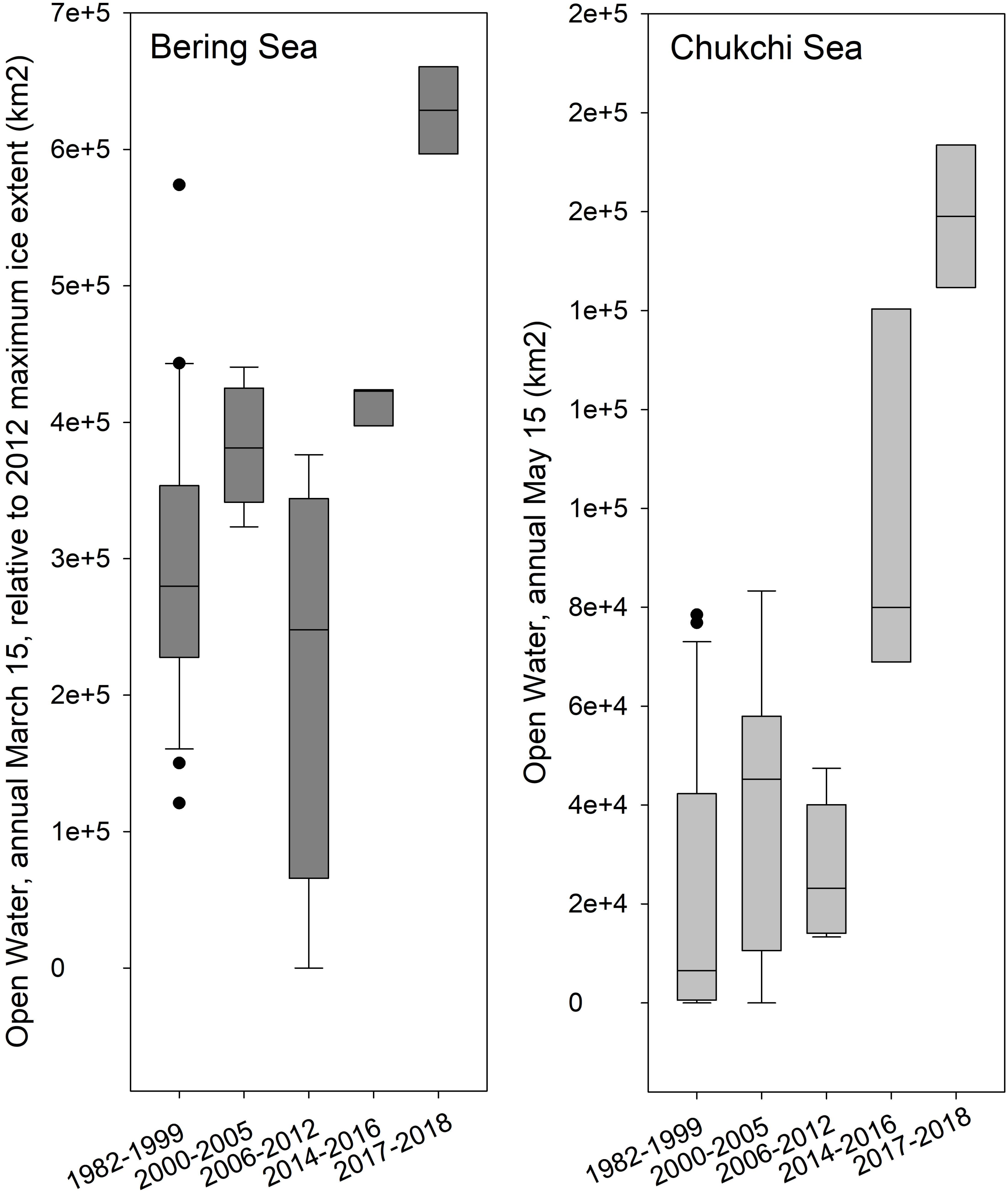
Bering Sea
Open Water, annual March 15, relative to 2012 maximum ice extent (km2)
7e+5
6e+5
5e+5
4e+5
3e+5
2e+5
1e+5
0
1982-1999
2000-2005
2006-2012
2014-2016
2017-2018
Chukchi Sea
Open Water, annual May 15 (km2)
2e+5
2e+5
2e+5
1e+5
1e+5
1e+5
8e+4
6e+4
4e+4
2e+4
0
1982-1999
2000-2005
2006-2012
2014-2016
2017-2018

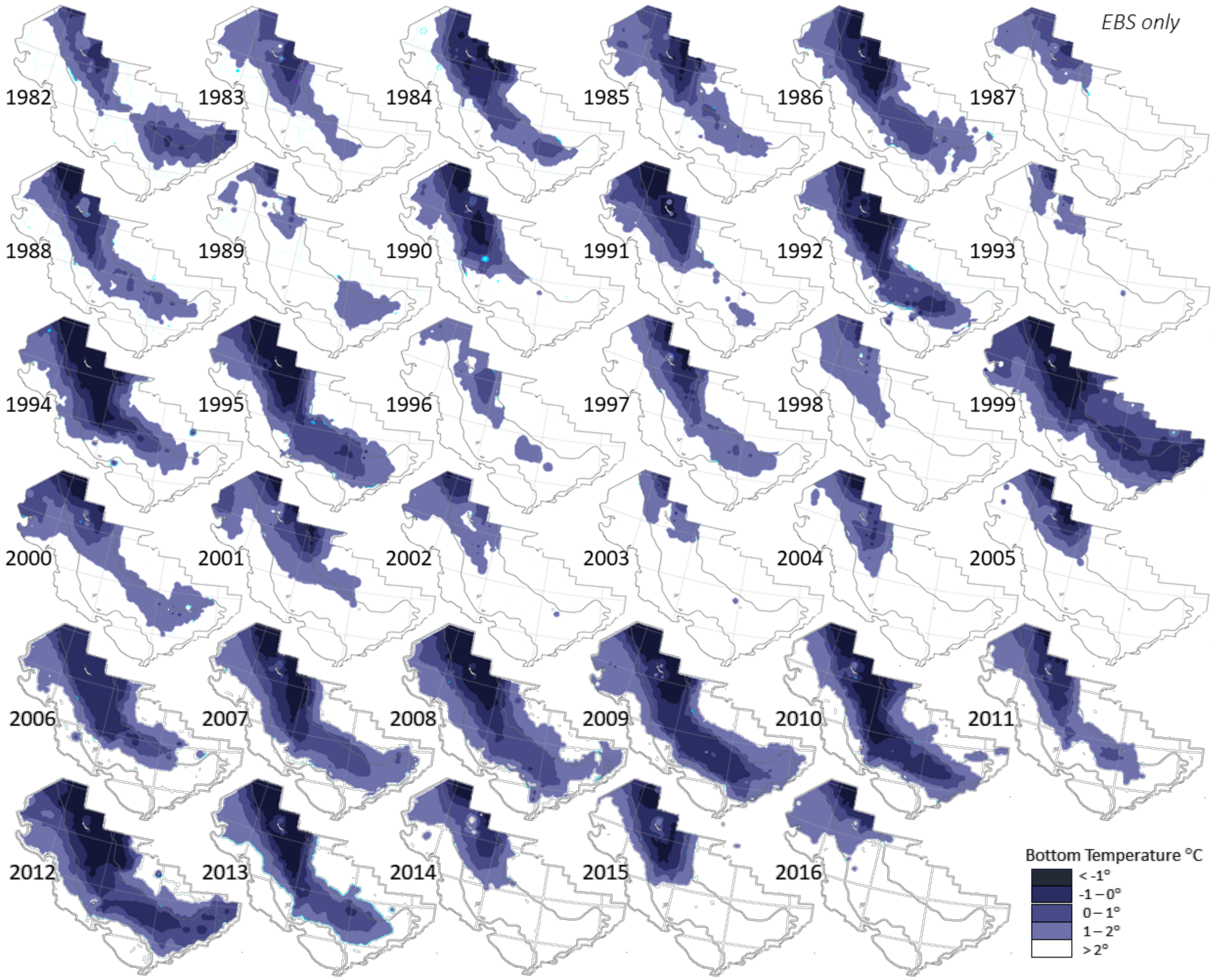
EBS only
1982
1983
1984
1985
1986
1987
1988
1989
1990
1991
1992
1993
1994
1995
1996
1997
1998
1999
2000
2001
2002
2003
2004
2005
2006
2007
2008
2009
2010
2011
2012
2013
2014
2015
2016
Bottom Temperature °C
< -1°
-1 – 0°
0 – 1°
1 – 2°
> 2°

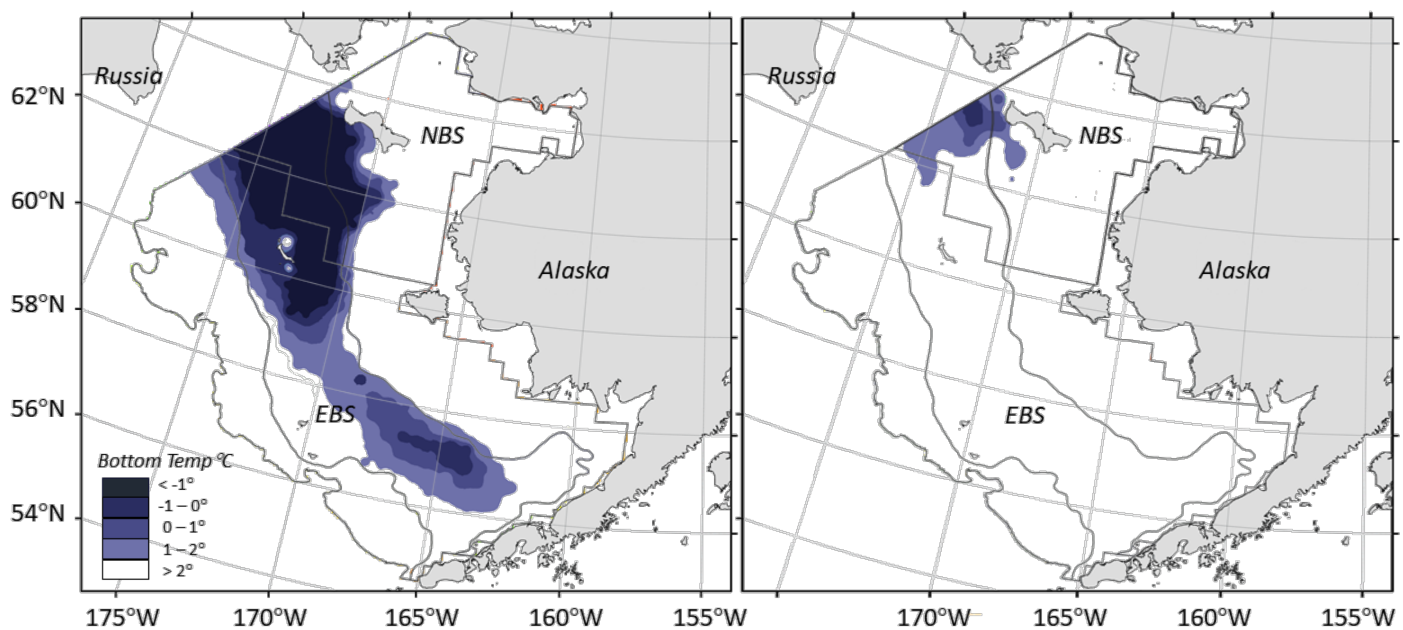
Russia
NBS
Alaska
EBS
62°N
60°N
58°N
56°N
54°N
Bottom Temp °C
< -1°
-1 – 0°
0 – 1°
1 – 2°
> 2°
175°W
170°W
165°W
160°W
155°W
Russia
NBS
Alaska
EBS
170°W
165°W
160°W
155°W

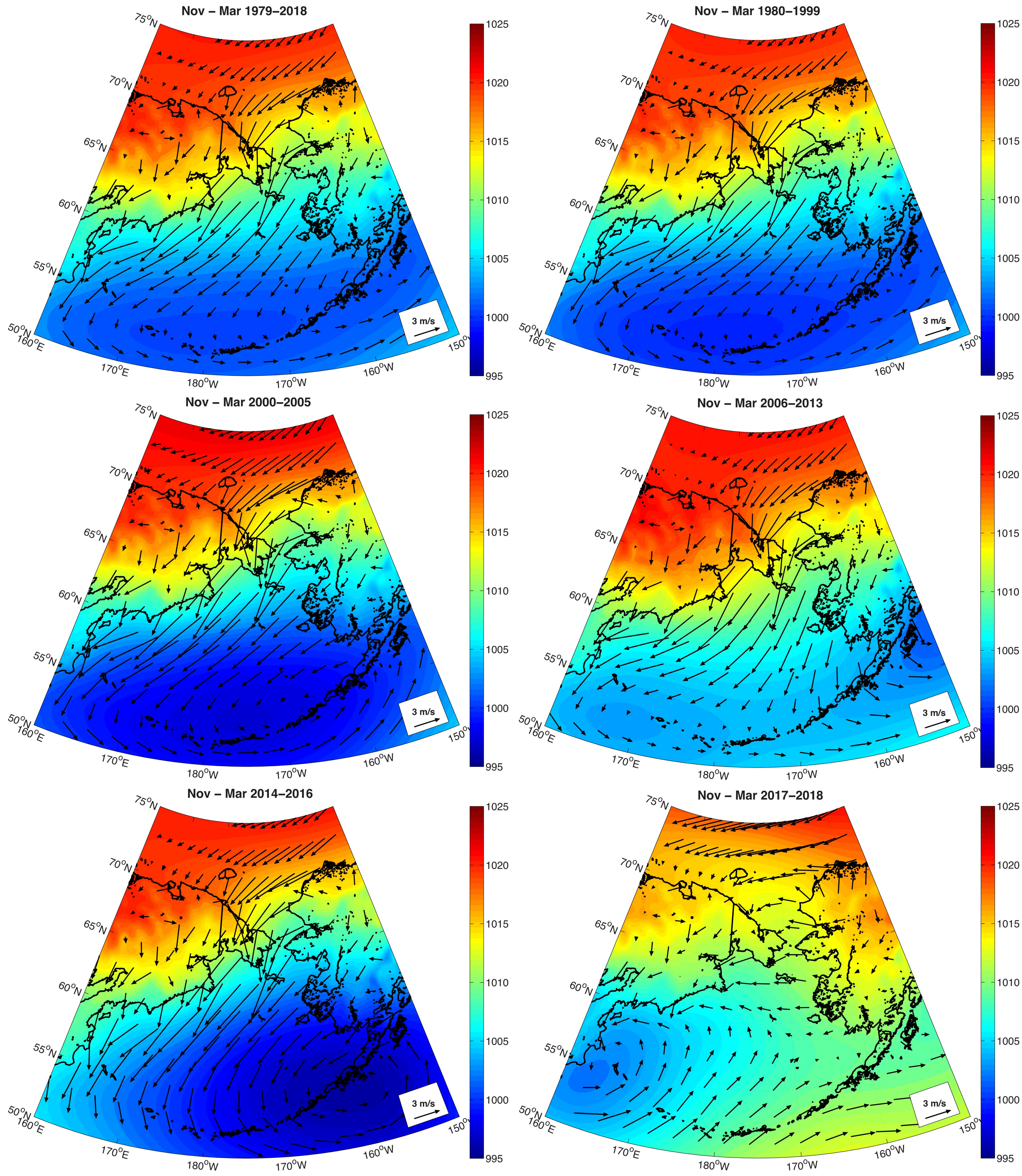
Nov – Mar 1979–2018
Nov – Mar 1980–1999
Nov – Mar 2000–2005
Nov – Mar 2006–2013
Nov – Mar 2014–2016
Nov – Mar 2017–2018
75°N
70°N
65°N
60°N
55°N
50°N
160°E
170°E
180°W
170°W
160°W
150°
3 m/s
1025
1020
1015
1010
1005
1000
995

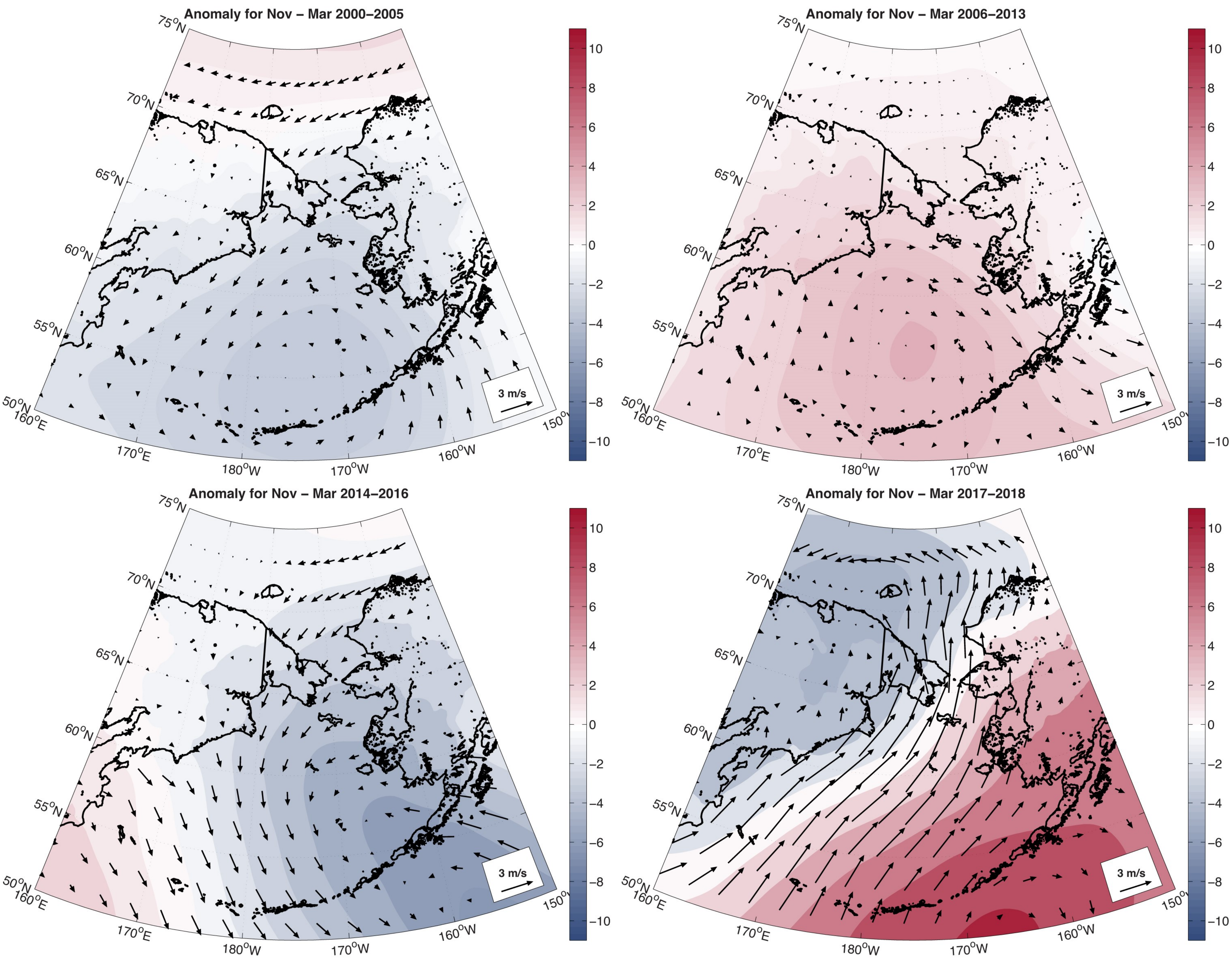

Anomaly for Nov – Mar 2000–2005
Anomaly for Nov – Mar 2006–2013
Anomaly for Nov – Mar 2014–2016
Anomaly for Nov – Mar 2017–2018
75°N
70°N
65°N
60°N
55°N
50°N
160°E
170°E
180°W
170°W
160°W
150°W
3 m/s
10
8
6
4
2
0
−2
−4
−6
−8
−10